Eur. Phys. J. C 1, 375–393 (1998)

THE EUROPEAN PHYSICAL JOURNAL C

Virtual LSPs at e^+ e^- colliders

Amitava Datta[1], Aseshkrishna Datta[1], Sreerup Raychaudhuri[2,*]

[1] Department of Physics, Jadavpur University, Calcutta 700 032, India
[2] Theoretical Physics Group, Tata Institute of Fundamental Research,
Homi Bhabha Road, Mumbai 400 005, India (e-mail: sreerup@theory.tifr.res.in)

Received: 20 May 1996 / Revised version: 19 March 1997

Abstract. Currently popular search strategies for supersymmetric particles may be significantly affected due to relatively light sneutrinos which decay dominantly into invisible channels. In certain cases the second lightest neutralino may also decay invisibly leading to two extra carriers of missing energy (in addition to the lightest supersymmetric particle (LSP)) – the virtual LSPs (VLSPs). A tree lavel calculation shows that if the sneutrino mass happens to be in the small but experimentally allowed range ($m_{\tilde{\nu}} \approx$ 45-55 GeV), these particles together with neutralino pairs may contribute significantly to the missing energy in the process $e^+e^- \longrightarrow \gamma + \not{E}$ at LEP-2 energies as an enhancement over the Standard Model or the conventional MSSM predictions. It is further shown that a much larger region of the parameter space can be scanned at a high luminosity e^+e^- collider at 500 GeV like the proposed NLC machine. Moreover, at both LEP-2 and NLC this process may play a complementary role to direct chargino searches, which may fail due to a near mass degeneracy of the chargino and the sneutrino. Formulae for the cross sections taking into account full mixings of the charginos and the neutralinos are derived. The signal remains observable even in the context of more restricted models based on N=1 SUGRA with common scalar and gaugino masses. A preliminary study of the QED radiative corrections due to soft multiple photon emission as well as hard collinear bremsstrahlung indicates that these corrections play a crucial role in estimating the background.

1 Introduction

It is well known that supersymmetry (SUSY) [1] is an attractive alternative to the Standard Model (SM) since it offers an elegant solution of the notorious naturalness problem, provided the masses of the superpartners are of the order of 1 TeV or less. The search for SUSY at the TeV scale is, therefore, a high-priority programme of current high energy physics. Extensive searches for SUSY at the present high energy accelerators including the Fermilab Tevatron and LEP-1 and LEP-1.5 have yielded negative results and have eliminated certain regions of the parameter space of the Minimal Supersymmetric extension of the Standard Model (MSSM)[1].

However, there are small but interesting regions of the parameter space, which are allowed by all experimental data, where the signatures of SUSY can be significantly different from the conventional ones considered in most cases. As an example, let us note that in most cases the search strategies for R-parity conserving SUSY particles are based on the assumption that there is a single, stable, weakly-interacting neutral superparticle, the so-called lightest supersymmetric particle(LSP). This particle, if produced, easily escapes detection and carries missing energy ($\not{E}$). Moreover, as a result of R-parity conservation, all other superparticles decay into the LSP either directly or through cascades. Thus any sparticle production is accompanied by $\not{E}$, traditionally regarded as the most powerful weapon in the arsenal of SUSY hunters, carried by the LSP alone.

It has been emphasised in recent literature [2,3] that in some interesting regions of the parameter space of the MSSM (with R-parity conservation) there could be other carriers of missing energy in addition to the LSP, due to sparticles which decay dominantly into invisible modes. In such a scenario the signals of sparticle production can be considerably different from the conventional ones. This happens in the following scenario.

The MSSM contains four spin-$\frac{1}{2}$ neutral electroweak gauginos. These particles are the superpartners of the photon, the Z-boson and the two neutral CP-even Higgs bosons. Linear combinations of these four states, the four neutral gauginos or neutralinos ($\widetilde{N}_i$, i=1,4), are the physical states. In the currently favoured models, the lightest neutralino($\widetilde{N}_1$) is assumed to be the LSP [1]. Similarly, linear combinations of the superpartners of the W-boson and the charged Higgs boson give two physical charged gauginos or charginos.

The usual assumption that the MSSM is embedded into some Grand Unified Theory (GUT) immediately implies, irrespective of the choice of any particular gauge group for the GUT, that the masses and the couplings of charginos and neutralinos depend only on three indepen-

dent parameters. Usually these are taken as $\mu, \tan\beta$ and the gluino mass $m_{\tilde{g}}$.

If no further assumption is made then the masses of the sfermions are totally independent of the gaugino-masses (we shall discuss below more restricted models with additional theoretical assumptions). Thus the sneutrinos ($\tilde{\nu}$, the superpartners of the neutrinos), though heavier than the LSP, could very well be lighter than the lighter chargino ($\widetilde{\chi}_1^{\pm}$), the second lightest neutralino ($\widetilde{N}_2$) and other superparticles. As a consequence, the invisible two-body decay mode $\tilde{\nu} \longrightarrow \nu\widetilde{N}_1$ opens up and completely dominates over the others, being the only kinematically-allowed two-body decay channel for the sneutrinos. The other necessary condition for this scheme to work is that the $\widetilde{N}_1$ has a substantial zino (superpartner of the Z-boson) component. This, however, is almost always the case as long as the gluino ($\tilde{g}$, the superpartner of the gluon) has a mass ($m_{\tilde{g}}$) in the range interesting for the SUSY searches at the Tevatron [4]. Moreover, in such cases the $\widetilde{N}_2$ — which also has a dominant zino component — decays primarily through the process $\widetilde{N}_2 \longrightarrow \nu\tilde{\nu}$. This, however, also requires the left and the right handed sleptons($\tilde{l_L}$ and $\tilde{l_R}$, the superpartners of leptons) to be heavier than $\widetilde{N}_2$. These two particles ($\widetilde{N}_2$ and $\tilde{\nu}$), decaying primarily into invisible channels, may act as additional sources of $\not{E}$ and can significantly affect the strategies for SUSY searches [2,3]. They are, therefore, called *virtual* or *effective* LSPs (VLSPs or ELSPs) [2,7] in the context of SUSY searches.

Some consequences of the VLSP scenario (as opposed to the conventional MSSM where the LSP is the only source of missing E) in the context of SUSY search at both hadron and $e^+\,e^-$ colliders have already been discussed in the literature [2,3,5–7]. Here we wish to reiterate that for LEP experiments beyond the Z-pole the predictions of the VLSP scenario are significantly different from the conventional ones. For example, experiments at LEP-1.5 [8] have recently reported some improved bounds on the chargino-neutralino sector. These bounds are derived from the processes (a) $e^+e^- \longrightarrow \widetilde{N}_1\widetilde{N}_2$ and (b) $e^+e^- \longrightarrow \widetilde{\chi}_1^+\widetilde{\chi}_1^-$, assuming that $\widetilde{\chi}_1^{\pm}$ and $\widetilde{N}_2$ primarily decay into 3-body channels as predicted by the conventional MSSM. In the VLSP scenario, however, the final state of process (a) is invisible. Thus the improved bounds on the neutralino sector from LEP-1.5 are not applicable in this scenario. Similarly in the presence of light $\tilde{\nu}$-s, $\widetilde{\chi}_1^{\pm}$ primarily decays (with branching ratio $\simeq$1) into the hadronically quiet channel $l^{\pm}\tilde{\nu}$ [2,5,7]. Thus the bounds on the chargino sector derived from the absence of events containing acoplanar jets and leptons and missing energy may have to be revised in this scenario. It will be interesting to use the absence of two acoplanar leptons in the above experiments to constrain the ($M_{\widetilde{\chi}_1^{\pm}} - m_{\tilde{\nu}}$) mass plane in the VLSP scenario. In principle the constraints on $m_{\tilde{e}_L}$ can also constrain $m_{\tilde{\nu}}$ for given $tan\beta$ (see Sect. 2, 2nd paragraph). The published limits are, however, are not very stringent at this moment [8]. However the constraints thus obtained will depend on $M_{\widetilde{\chi}_1^{\pm}}$ - $m_{\tilde{\nu}}$ and can be completely evaded if $\tilde{\nu}$ and $\widetilde{\chi}_1^{\pm}$ are nearly degenerate so that the leptons in the final state are soft and unobservable.

Of course in some channels the signal may turn out to be identical in both scenarios. The slepton pair production is a case in point. The dominant decay mode of the sleptons is likely to be $l + \widetilde{N}_1$ even in the presence of VLSPs. SUSY may very well be discovered through such a channel. Still it is therefore important to identify signals which can distinguish the VLSP scenario from the conventional MSSM.

In this paper we consider one such process $e^+e^- \longrightarrow \gamma$ +nothing($\not{E}$) at the tree level. This was already discussed in a previous letter [6] in the context of **LEP-2** only. Here we shall discuss the signal both at LEP-2 and at other future e^+e^- colliders at higher energies. In the SM only $\nu\overline{\nu}$ pairs contribute to the final state. In the conventional MSSM both $\nu\overline{\nu}$ and $\widetilde{N}_1\widetilde{N}_1$ pairs contribute to this final state. With VLSPs, however, there will be additional contributions from $\tilde{\nu}\tilde{\overline{\nu}}$ and $\widetilde{N_i}\widetilde{N_j}$ ($i,j = 1,2$) which tend to increase the cross section quite significantly. In [6] it was found that a significant enhancement of the cross section over the prediction of the SM occurs at LEP-2 in a reasonable region of the MSSM parameter space (see Sect. 2 for further details) already constrained by the experimental data (most notably from LEP-1 [9]). Moreover, the bulk of the extra contribution comes from $\tilde{\nu}\tilde{\overline{\nu}}$ pairs. Thus, such a signal, if detected, can be distinguished not only from the SM but also from the conventional MSSM without VLSPs. An additional attractive feature of this channel is that it may lead to a visible signal even if the charginos and the sneutrinos are almost mass degenerate.

In this work we have elaborated the results of [6] with further details. The scan over the LEP-1 allowed parameter space is now more complete. This, however, does not alter the results of [6] qualitatively, although some quantitative changes are noted. As in [6] we have found that at LEP-2 the statistical significance of the signal is rather modest. For optimistic choices of SUSY parameters(most notably for relatively low sneutrino and gluino masses, $m_{\tilde{\nu}}$= 45—60 GeV, $m_{\tilde{g}} \simeq$ 200GeV), the tree level cross sections yield signals with statistical significance $\geq 3\sigma$ (numerical details are given in the next section).

The tree level cross sections for the process $e^+e^- \longrightarrow \gamma + nothing(\not{E})$ have been discussed extensively in the literature. We have done a complete calculation in the VLSP scenario without using the simplifying assumptions used in earlier works. In [6] we presented some of the numerical results. But the formulae for the cross sections, which are quite cumbersome, could not be presented in a brief letter. A major result of this paper is the detailed formulae presented in a compact form.

First we have calculated the full cross section for the purely SM process $e^+e^- \longrightarrow \gamma\nu\bar{\nu}$. In many of the earlier works [10], appropriate for LEP-1, the contribution of the W-exchange diagrams was computed in the limit of four-fermion contact interaction. We have recalculated it with the full W-propagator. We have also taken the widths of W and Z into account. Our results agree completely with those of [10] after taking the appropriate limits. In [11] this

cross section was also computed without any approximation. However, the published results include several misprints (see, for example, (3) which contains several terms which are dimensionally incorrect). This makes comparison rather difficult. Further comments on this discrepancy will be made in Sect. 2. This cross section was also computed in [12] by neglecting the widths but keeping the full W-propagator. Their analytical formulae agree completely with ours in the appropriate limit. Moreover, a comparison of the numerical results shows that effects of the widths are indeed negligible, at least for the energy ranges considered in this paper.

The most important contribution to this process in the VLSP scenario comes from $e^+e^- \longrightarrow \gamma\tilde{\nu}\bar{\tilde{\nu}}$. Only the amplitudes of the relevant Feynman diagrams are given in, for example, [13] in the limit when the chargino is purely a wino (superpartner of the W-boson). We have computed the full cross section taking into account the chargino-mixing matrix. Our numerical results agree with those of [13] in the appropriate limit. In a more recent paper [14] this cross section has been computed by assuming the charginos to be very massive. In this limit we agree with the main features of their results.

We have also computed the cross section for the process $e^+e^- \longrightarrow \gamma\widetilde{N}_i\widetilde{N}_j$, $(i,j = 1,2)$ taking the 4×4 neutralino mass matrix into account. This cross section with only LSP-pairs ($i = j = 1$) in the final state is also relevant for the conventional MSSM and was computed in [15] in the limit when the $\widetilde{N}_1$ is a pure photino without any mixing. In this approximation the s-channel Z-exchange diagrams are absent which reduces the number of diagrams and interferences between them. Our numerical results agree, in the appropriate limit, with the those of [15]. In a recent paper [16] the calculation for a mixed LSP has been done using the structure function approach [17]. One of the conclusions of [6], *viz.* LSP pairs alone cannot give a signal with acceptable statistical significance, is supported by [16]. The general formulae presented in this paper also include the contributions of $\widetilde{N}_1\widetilde{N}_2$ and $\widetilde{N}_2\widetilde{N}_2$ pairs.

In Appendix-A we present analytical formulae for all the matrix elements squared.

Using these results we have also computed the cross sections at $e^+\,e^-$ colliders at higher energies after introducing kinematical cuts to reduce the SM backgrounds. Many of these machines are likely to be of very high luminosities [18]. As a consequence of this, signals of very high statistical significance ($> 5\sigma$) can be obtained at CM energies ≈350 and 500 GeV which are attainable at the proposed Next Linear Collider(NLC). Special care, however, should be taken to reduce the background from radiative Bhabha scattering where both the final state charged particles are lost in the beam pipe [14]. This will be discussed in further details in Sect. 3.

The VLSP scenario, which is certainly consistent with all available experimental results on SUSY searches, can also be accommodated in the more constrained and theoretically motivated models based on $N = 1$ Supergravity with common scalar and gaugino masses at a high scale [19]. In this scenario the sneutrino and the gaugino masses are not completely independent, but get related through the renormalisation group (RG) equations. It was shown in [7] that the VLSP scenario can be accommodated even in this highly constrained scenario. In this paper we have found that the signal at LEP-2 is reasonable for certain regions of the parameter space given in [7], while at NLC, signals with high statistical significance can still be obtained.

It may be noted at this point that in [6] only the lowest order cross section was considered. In this paper we have included the effects of soft multiphoton emission and hard collinear bremsstrahlung on the cross section. These effects can be studied by using, e.g., the structure function approach of [17]. Our preliminary analysis indicates that the impact of these corrections on the background is nontrivial and further studies including all QED and electroweak corrections are called for.

The plan of the paper is as follows. In Sect. 2 we consider the signal at $\sqrt{s}$=190 GeV corresponding to the LEP-2 energies and briefly comment on the possibilities at LEP-1.5. In Sect. 3 the same discussion is carried out for high luminosity e^+e^- colliders operating at higher energies. In Sect. 4 the signal is discussed in the context of highly constrained models based on $N = 1$ SUGRA. Section 5 discusses briefly the effects of certain QED corrections on the signal. Our conclusions are summarised in Sect. 6. The relevant formulae for the cross sections are given in the Appendix.

2 The signal at LEP-2 energies

In our calculations we use the usual assumption of a common gaugino mass at the GUT scale which relates the $U(1)$ gaugino mass M_1 with the $SU(2)$ gaugino mass M_2 [1]. With this assumption M_2, the higgsino mass parameter μ and $\tan\beta$ determine the masses and the couplings of the charginos and neutralinos completely. In some of our figures we have used $3M_2$ as the variable instead of M_2. The advantage is that this is approximately equal to the running gluino mass (through the above assumption of unification) which can be directly related to the constraints obtained from the Tevatron [4]. We, however, emphasise that this equality is only approximate and the factor 3 may change, though not drastically, with the energy scale. Nevertheless we shall denote in the following $3M_2$ by the gluino mass ($m_{\tilde{g}}$) for the sake of simplicity.

In addition we have assumed the $SU(2)$ breaking relation:

$$m_{\tilde{l}_L} \;=\; \sqrt{m_{\tilde{\nu}}^2 \;+\; \cos^2\theta_W \, D_Z}$$

where

$$D_Z \;=\; M_Z^2 \, \frac{\tan^2\beta - 1}{\tan^2\beta + 1}$$

and $m_{\tilde{\nu}}$ is treated as a free parameter and three degenerate sneutrinos are assumed. For the right handed sleptons we have made the popular assumption $m_{\tilde{l}_R} \approx m_{\tilde{l}_L}$ although deviations from this approximation may naturally occur in some models.

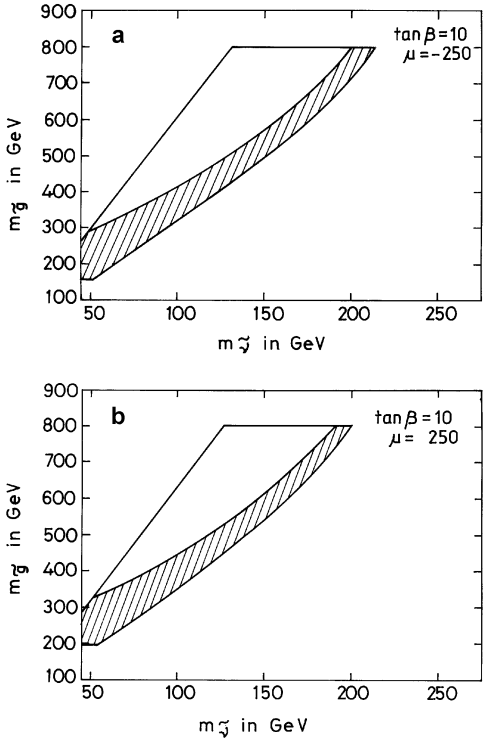

Fig. 1. The region in the $m_{\tilde{\nu}} - m_{\tilde{g}}$ plane compatible with the VLSP scenario with tanβ =10 for **a** $\mu = -250$ and **b** 250 GeV (see Sect. 2 for further explanations). We have used $m_{\tilde{g}} \approx 3M_2$ (see Sect. 2, paragraph 1)

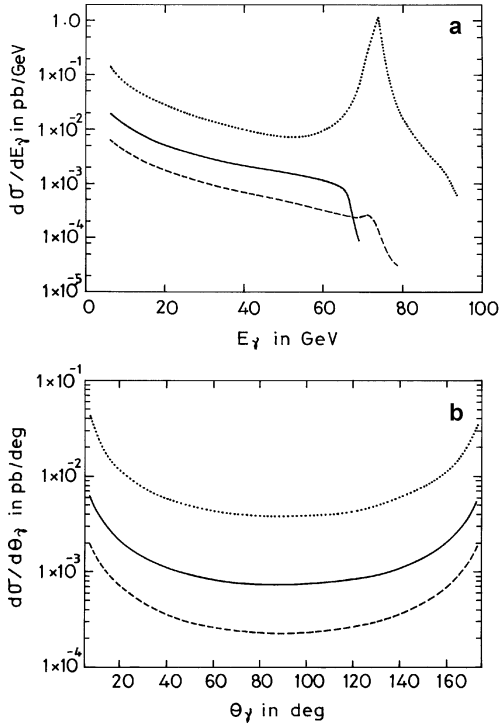

Fig. 2. a Energy distribution of the photon at $\sqrt{s}$ =190 GeV, with $E_\gamma > 5$ GeV and $5^\circ < \theta_\gamma < 175^\circ$. **b** Angular distribution of the photon at $\sqrt{s}$ =190 GeV with 5< E_γ <60 GeV and $5^\circ < \theta_\gamma < 175^\circ$. The convention for different lines and SUSY parameters chosen are explained in Sect. 2

In the VLSP scenario the following constraints must be satisfied [7]:

$$m_{\tilde{\nu}} < M_{\widetilde{N}_2} < m_{\tilde{l}_L}, m_{\tilde{l}_R}$$
$$m_{\tilde{\nu}} < M_{\widetilde{\chi}_1^\pm} < m_{\tilde{l}_L}$$

In Figs. 1a and 1b we present the regions in the $(m_{\tilde{g}} - m_{\tilde{\nu}})$ mass plane (where the precise definition of the parameter $m_{\tilde{g}}$ is given in the first paragraph) compatible with the above inequalities for $\mu = -250$ (Fig. 1a) or +250 (Fig. 1b) GeV, tanβ=10, 150 GeV $\leq m_{\tilde{g}} \leq$ 800 GeV and $m_{\tilde{e}_L} = m_{\tilde{e}_R}$. In each figure the entire bounded area corresponds to the region of the parameter space where $\tilde{\nu}$-s behave like VLSP-s. Corresponding to each $m_{\tilde{\nu}}$, this happens for a range of $m_{\tilde{g}}$. The lower limit of this range comes from the condition $m_{\tilde{\nu}} < M_{\widetilde{N}_2}, M_{\widetilde{\chi}_1^\pm}$ while the upper limit comes from $M_{\widetilde{N}_1} < m_{\tilde{\nu}}$. If the additional condition $M_{\widetilde{N}_2} < m_{\tilde{e}_L}, m_{\tilde{e}_R}$ is satisfied then $\widetilde{N}_2$ also decays invisibly. This happens in the shaded region of the figures. The area of this region, however, is crucially dependent on the choice $m_{\tilde{e}_L} \approx m_{\tilde{e}_R}$. If $m_{\tilde{e}_R}$ is reduced, the shaded areas may shrink further. From Figs. 1a and 1b it is also apparent that the allowed region is almost independent of the choice of μ unless μ is very small. Small values of μ are, however, disfavoured by data from LEP-1.

As discussed in the introduction, the processes (**A**) $e^+e^- \longrightarrow \widetilde{\nu}\bar{\widetilde{\nu}}\gamma$, (**B**) $e^+e^- \longrightarrow \widetilde{N}_1\widetilde{N}_1\gamma$ and (**C**) $e^+e^- \longrightarrow \widetilde{N}_1\widetilde{N}_2\gamma$ contribute to the signal at $\sqrt{s} = 190$ GeV. At this energy the contribution of $e^+e^- \longrightarrow \widetilde{N}_2\widetilde{N}_2\gamma$ is indeed negligible. We have scanned over the entire LEP-1 allowed parameter space compatible with the VLSP scenario and have computed the cross sections from the processes **A** and **B**. In this section we shall restrict ourselves to tree level cross sections only. If, for a particular choice of the parameters, $\widetilde{N}_2$ is also a VLSP (the shaded region in Figs. 1a and 1b) then the contribution from the process **C** is also taken into account.

We show in Fig. 2a the energy distribution of the photon for processes **A**(the solid line) and **B**(the dashed line). Photons in the forward direction (those emitted within an angle of 5° with the beam axis) are not considered. There is a mild cut $E_\gamma > 5$ GeV which in conjunction with the strong angular cuts(discussed below) removes other backgrounds including the ones from radiative Bhabha scattering with the final state e^+e^- pair going down the beam pipe. This cut also takes into account the detector threshold. The SUSY parameters used are $m_{\tilde{\nu}} = 50$ GeV, $m_{\tilde{e}_L} = m_{\tilde{e}_R}$, $m_{\tilde{g}} = 200$ GeV, $\mu = -200$ GeV and tanβ= 5.

The main SM background comes from the process **(D)** $e^+e^- \longrightarrow \nu\bar{\nu}\gamma$. The corresponding distribution (the dotted line) for this background is also shown in Fig. 2a. As has already been discussed in [6], this distribution has a peak at about $(s - M_Z^2)/2\sqrt{s}$ corresponding to the decay of a real Z into $\nu\bar{\nu}$, as expected. Thus an upper cut of

Table 1. The comparison of the response of the signal to two sets of cuts **A**[6] and **B**[15] at $\sqrt{s}$=190 GeV where Cut **A** $\equiv$ 5< E_γ <60 GeV, 40° < $\theta\gamma$ < 140°; Cut **B** $\equiv$ 6.175< E_γ <47.5 GeV, 18° < $\theta\gamma$ <162°, p_{T_γ} >6.175 GeV. Other fixed values of the SUSY parameters used are $(\mu, m_{\tilde{g}}, \tan\beta)$=(−300 GeV, 200 GeV, 10) and $m_{\tilde{e}_L} = m_{\tilde{e}_R}$. The SM background with Cut **A**(**B**) is 0.45(0.51)pb. All masses are in GeV and cross-sections are in picobarns. The statistical significance σ is computed for an integrated luminosity($\mathcal{L}$) of 500 pb^{-1}

$m_{\tilde{\nu}}$	Cut	$\sigma_{\tilde{\nu}\tilde{\nu}}$	$\sigma_{\widetilde{N}_1\widetilde{N}_1}$	$\sigma_{\widetilde{N}_1\widetilde{N}_2}$	Total	$\sigma = \frac{S}{\sqrt{B}}$
45	**A**	.103	.027	.018	.148	4.9
	B	.117	.031	.022	.170	5.3
55	**A**	.077	.025	.016	.118	3.9
	B	.087	.029	.019	.135	4.2
65	**A**	.048	.023	.015	.086	2.8
	B	.053	.026	.017	.096	3.0

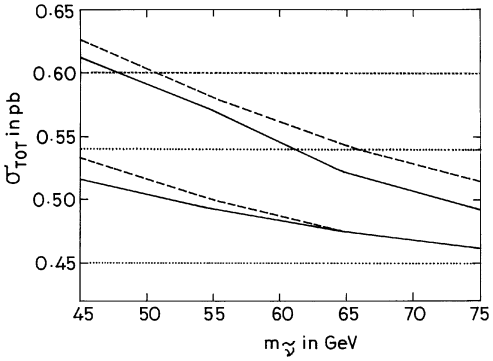

Fig. 3. The total cross section (SM+VLSP) as a function of $m_{\tilde{\nu}}$ at $\sqrt{s}$ =190 GeV. The band within the solid lines correspond to the SM+$\tilde{\nu}\tilde{\nu} + \widetilde{N}_1\widetilde{N}_1$ cross section and is obtained by varying $m_{\tilde{g}}$, μ and tanβ over the LEP-1 allowed region. The band within the dashed lines is obtained by taking additional contributions from $\widetilde{N}_1\widetilde{N}_2$ pairs into account. The horizontal dotted lines correspond to the SM background and its fluctuations (see Sect. 2)

E_γ <60 GeV optimises $\sigma = \frac{S}{\sqrt{B}}$ where S is the number of signal events and B is the number of background events.

In Fig. 2b we present the angular distribution of the signal (for the above SUSY parameters) and the background following the conventions of Fig. 2a. The distributions have similar characteristics. Thus angular cuts cannot further improve the quality of the signal. An irreducible background therefore remains.

Since we are not in a position to carry out detector simulations, we have introduced cuts in such a way that only signal collected in the central part of the detector is considered. This, in our opinion, gives a conservative assessment of the prospect of discovering the signal. We impose an angular cut $40° < \theta_\gamma < 140°$, where θ_γ is the angle between the photon and the direction of the positron. This cut corresponds to the high p_T photons collected in the central part of the detector where photon detection efficiency is expected to be large (≈ 1). We have also studied the effects of a cut allowing for more angular coverage alongwith an explicit strong cut on the p_T of the photon to remove the Bhabha background. These cuts, introduced in a recent paper [16], are given by $18° < \theta_\gamma < 162°$, $6.175 < E_\gamma < 47.5$ GeV and $p_{T_\gamma} > 6.175$ GeV. Now the photons detected in the endcap region of the detector also contribute and it is assumed that their detection efficiency is still large (≈ 1). We compare the response of the signal for the two sets of cuts in Table 1 and find that they give very similar results. Using our cuts the background is 0.45 pb while for the cuts of [16] it is 0.51 pb.

It is to be noted that the second number is considerably smaller than the result quoted in [16] ($\approx$ 0.87 pb). Since the background estimate is crucially important for assessing the observability of our signal, which is rather modest, we have looked into this discrepancy in further details.

The difference stems from the fact that in [16] the cross section was computed by using the formulae of [11]. As mentioned in the introduction, there are several terms in the matrix element of [11] (see (3)) which are dimensionally incorrect. These terms, however, correspond to the diagram 5 of Fig. 11 of our paper. The amplitude in this case is suppressed by two W-propagators and is numerically small. There are, however, other important disagreements. Our result for the interference of the two t-channel diagrams [(3) and (4) of Fig. 11] does not agree with (3) of [11]. We have checked that this contribution is numerically quite significant.

For numerical computations, however, (7) of [11], which is obtained from (2) and (3) after dropping the above dimensionally incorrect terms, was recommended. We have convinced ourselves that (7) still contains the discrepancy regarding the interference terms as discussed in the last paragraph. In the last paper of [17], which uses the matrix element of [11], the W and $W - Z$ interference contributions were plotted separately (see Fig. 4b). We have checked that this plot can be easily reproduced from (3) of [11] which is controversial. As a result, the disagreement between the above figure and our result is considerable. On the other hand the pure Z exchange contributions as obtained in [17] (see Fig. 4a) and [11] completely agree with ours. In order to improve the signal to background ratio we have imposed cuts as discussed above. The main purpose of these cuts is to reduce the Z contribution to the background. After these cuts the relative weights of the W and $W - Z$ interference terms in the background cross section increases. This is responsible for the significant disagreement between the background estimates of [16] and ours.

We, however, prefer to use the numbers derived from our formulae which agree algebraically with those of [12] in the limit Γ_W=0. Moreover, the numerical changes due to $\Gamma_W \neq 0$ are negligible.

In Fig. 3 we present the cross section as a function of $m_{\tilde{\nu}}$ for $m_{\tilde{e}_L} = m_{\tilde{e}_R}$ with our conservative cuts. Throughout this section we shall take the integrated luminosity $\mathcal{L}$ =500 pb^{-1}.

The strongest limit on the sneutrino mass $m_{\tilde{\nu}}$ >43.6 GeV comes from the width of Z for invisibly decaying

sneutrinos. We have however taken $m_{\tilde{\nu}}$ >45 GeV. In this case only the LSPs contribute to the invisible width. We have not scanned the narrow region 43.6< $m_{\tilde{\nu}}$ <45 GeV. But it is unlikely that this will affect our conclusions seriously. The points in the $m_{\tilde{g}} - \mu - tan\beta$ parameter space are now chosen for each $m_{\tilde{\nu}}$ by considering the constraints from LEP-1. We remind the reader that we use $m_{\tilde{g}} \approx 3M_2$ for reasons discussed at the beginning of this section. The most important ones are $M_{\widetilde{\chi}_1^{\pm}}$ >46 GeV, $\Gamma(Z \rightarrow \widetilde{N}_1\widetilde{N}_1)$ <8.4 MeV, $Br(Z \rightarrow \widetilde{N}_i\widetilde{N}_j)$ ≃a few times 10^{-5}, $\Gamma(Z \rightarrow$ nonstandard particles)¡23.1 MeV. Out of the allowed range we have chosen 200≤ $m_{\tilde{g}}$ ≤400, −500≤ μ ≤ 500, 2≤ $tan\beta$ ≤30. This scanning of the parameter space is more comprehensive than the one carried out in [6].

The choice $m_{\tilde{g}}$ ≥200 GeV is guided by the limits on $m_{\tilde{g}}$ from direct searches at the Tevatron. Unfortunately this limit depends on the squark mass($m_{\tilde{q}}$). We note that $m_{\tilde{g}} < 212$ GeV is ruled out from SUSY searches at Tevatron for $m_{\tilde{q}} \approx m_{\tilde{g}}$ [4]. For $m_{\tilde{q}} >> m_{\tilde{g}}$, the limit is $m_{\tilde{g}}$ >144 GeV. Strictly speaking these limits pertain to the pole mass of the gluino. However for $m_{\tilde{q}} \approx m_{\tilde{g}}$, the running gluino mass (the parameter more directly related to the chargino - neutralino sector through the assumption of unification) is equal to the pole mass to a very good approximation [22]. For $m_{\tilde{q}} >> m_{\tilde{g}}$, the difference between the above two masses is significant. In fact it turns out that in this case the above limit on $m_{\tilde{g}}$ translates into a much relaxed bound on the running gluino mass. Moreover these limits may reduce substantially in the VLSP scenario [23]. Since the squark mass is not otherwise an important parameter in this phenomenological analysis, we have not considered the lower edge of the allowed gluino mass spectrum which depends on the specific choice $m_{\tilde{q}} >> m_{\tilde{g}}$. We have taken $m_{\tilde{g}}$ ≥200 GeV , which, in our opinion, is a conservative choice. Sometimes, however, we shall take, mainly for the purpose of illustration, $m_{\tilde{g}}$ around 150 GeV which is allowed for heavy squarks. For $m_{\tilde{g}}$ ≥400 GeV the signal falls below the 2σ level and becomes uninteresting.

The band within the solid lines in Fig. 3 corresponds to the combined cross sections σ_{tot} from the processes **A**, **B** and **D**, i.e. the scenario in which the $\tilde{\nu}$ is the only VLSP. In order to obtain conservative estimates, we have not considered the possibility that $\widetilde{N}_2$ may also be a VLSP. This is because the latter possibility can be evaded by an appropriate choice of $m_{\tilde{e}_R}$. The width of this band is due to varying $m_{\tilde{g}}$, μ and tanβ within the above ranges and is a measure of SUSY parameter space consistent with the VLSP sceanrio for a given $m_{\tilde{\nu}}$. Taking into account the points where $\widetilde{N}_2$ is also a VLSP, for the choice $m_{\tilde{e}_L} = m_{\tilde{e}_R}$, the signal improves modestly due to the contribution from process **C** which is shown by the band enclosed by the dashed lines. For comparison we also display the cross section for the background (process **D**) which corresponds to the lowest dotted horizontal line in the figure. The other two dotted horizontal lines correspond to 3σ and 5σ fluctuations of the background events for an integrated luminosity of 500 pb^{-1}. From the figure it may be noted that a 5σ signal can be obtained for $m_{\tilde{\nu}}$ ≤52 GeV for a very small region of SUSY parameter space. A much larger region of parameter space gives events above 3σ fluctuation with $m_{\tilde{\nu}}$ ≤66 GeV. In this figure the upper edges of the bands correspond to $m_{\tilde{g}} = 200$ GeV and low tanβ (2≤tanβ ≤6). The cross section is rather insensitive to the variation of μ. For $m_{\tilde{g}} = 300$ GeV only 3σ signals can be obtained for a limited region of the parameter space while for $m_{\tilde{g}} = 400$ GeV the signal remains below the 2σ level for the entire region of the parameter space.

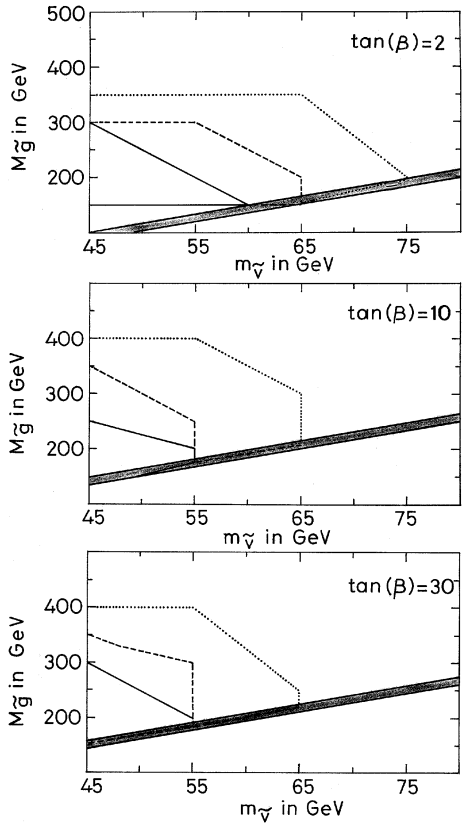

Fig. 4. Contour plots in the ($m_{\tilde{\nu}} - m_{\tilde{g}}$) plane at $\sqrt{s}$ =190 GeV indicating the regions where ≥2σ (*dotted*), ≥3σ (*dashed*) and ≥4σ (*solid*) signals may be obtained for tanβ = 2,10 and 30 and $-500 \leq \mu \leq 500$. The *shaded region* corresponds to $m_{\tilde{\nu}} < M_{\widetilde{\chi}_1^{\pm}} < m_{\tilde{\nu}} + 5$ GeV, where the direct chargino decay is likely to be difficult to detect. We have used $m_{\tilde{g}} \approx 3M_2$ (see Sect. 2)

However, before drawing a final conclusion on the statistical significance of the signal higher order corrections should be taken into account carefully. A preliminary discussion given in Sect. 5 indicates that they are indeed nontrivial.

A clearer representation of the regions in the ($m_{\tilde{g}} - m_{\tilde{\nu}}$) plane that can be probed at $\sqrt{s}$=190 GeV is given by the contour plot in Fig. 4 for three values of tanβ=2,10,30. The points within the solid, dashed and dotted contours yield signals with statistical significances ≥4σ, 3σ and 2σ respectively for suitable choices of μ. In addition to $m_{\tilde{g}}$ ≥200 GeV, we have also considered the region 150 GeV ≤ $m_{\tilde{g}}$ ≤200 GeV, since this region is still allowed by the Tevatron data for heavy squarks. The signal, however, is not considered for points where the VLSP constraints

discussed above are not satisfied. The shaded band corresponds to $M_{\tilde{\chi}_1^\pm} - m_{\tilde{\nu}} < 5$, where SUSY signals from direct chargino decays may be difficult to obtain.

Since experiments at LEP-1.5 are in progress, the cross section at $\sqrt{s}$ =130 GeV is of considerable interest. However, even for $m_{\tilde{\nu}}$ =50 GeV and other favourable choices of the SUSY parameters ($\mu = -300$, $m_{\tilde{g}}$ =200 and tanβ =5) the cross section happens to be rather disappointing. The total cross section of the processes **A**−**C** is 0.054 pb while the background is 0.373 pb with the cuts $5 < E_\gamma < 20$ GeV and $40^\circ < \theta_\gamma < 140^\circ$. Thus for an integrated luminosity of 6 pb^{-1} the statistical significance is certainly $< 3\sigma$.

From the above results it is clear that the process under consideration has a rather modest cross section at LEP. The bulk of the constraints in the chargino-sneutrino sector in the VLSP scenario is therefore likely to come from direct chargino searches [7]. Nevertheless this process is likely to play a complementary role in the regions of the parameter space where the chargino and the sneutrino are nearly degenerate and the sneutrino masses are relatively small. To illustrate this point we consider an example with $\mu = -350$ GeV, tan $\beta = 6$ and $m_{\tilde{g}} = 150$ GeV. In this case the chargino mass is 53 GeV. The total signal cross section for $m_{\tilde{\nu}} = 50$ GeV is 0.17 pb which corresponds to 5 σ. It can be readily checked that the signal is weaker for higher $m_{\tilde{g}}$s, i.e., for larger chargino - sneutrino mass differences. This reduction for higher $m_{\tilde{g}}$ is essentially due to propagator supression in process A) and due to kinematical effects in processes B) and C) and holds for other choices of SUSY parameters. Thus in contrast to the direct chargino searches, the regions of the parameter space where the chargino and the sneutrino are nearly mass degenerate can be probed via this mode, provided the sneutrinos are not too heavy. In Fig. 4 the shaded region corresponds to $m_{\tilde{\nu}} < M_{\tilde{\chi}_1^\pm} < m_{\tilde{\nu}}+5$ GeV, where the chargino decay is likely to be difficult to detect. The statistical significance of the signal cannot be judged directly from this figure for the entire shaded region. This is because we have not computed the cross sections for $m_{\tilde{g}} < 150$ GeV, since this region is either ruled out or marginally allowed by the Tevatron data depending on the assumption on the squark mass. The cross sections have also not been computed for parameters for which the VLSP condition is not satisfied. However in regions not excluded by these considerations, the cross section is significant. This is especially so for relatively large tan β.

3 The signal at NLC

In this section we discuss the signal and the background for e^+e^- collisions at **NLC** for two values of centre of mass energy *viz.* $\sqrt{s}$=350 GeV and $\sqrt{s}$=500 GeV.

For $\sqrt{s}$=350 GeV the energy and angular distributions of the radiated photon in the signal [process **(A)** and process **(B)**] and background [process **(D)**] are shown in Fig. 5a and Fig. 5b respectively. The set of SUSY parameters used are $m_{\tilde{\nu}}$=80 GeV and $m_{\tilde{g}}$=350, $\mu = -500$ and

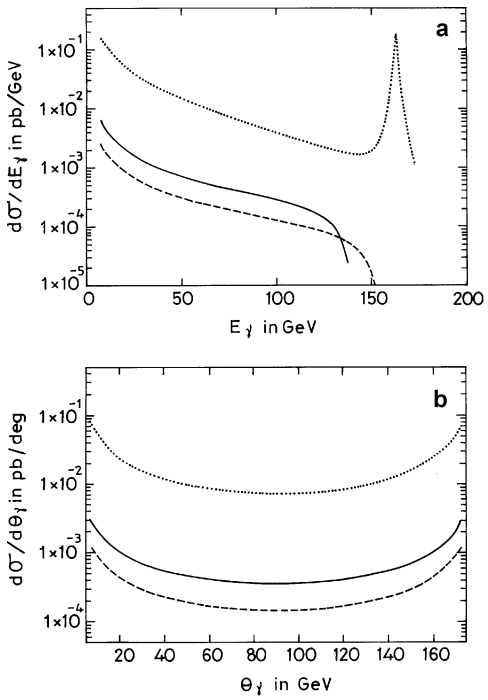

Fig. 5. a Energy distribution of the photon at $\sqrt{s}$ =350 GeV, with E_γ >5 GeV and $5^\circ < \theta_\gamma < 175^\circ$. **b** Angular distribution for the photon at $\sqrt{s}$ =350 GeV with $15 < E_\gamma < 150$ and $5^\circ < \theta_\gamma < 175^\circ$. The convention for different lines and SUSY parameters chosen are explained in Sect. 3

tanβ=5. The conventions for different curves are the same as those in Figs. 2a and 2b. The energy distribution (Fig. 5a) of the background has a peak at about $\sqrt{s}/2$ which is the beam energy. Thus an upper cut of E_γ <150 GeV is set.

A lower cut on the photon energy is set from naive kinematics of the background due to radiative Bhabha scattering which requires special care [14]. We have devised our cuts against this background assuming that e^+e^- scattered within a cone of 10° with respect to the beam axis may remain undetected. From kinematics we find that in this situation the photons are restricted by the following criteria: $E_\gamma \leq 65$ GeV, $p_{T_\gamma} \leq 52$ GeV. We have also checked that either of the above cuts reduces the Bhabha background completely. From the E_γ distribution (Fig. 5a) it is also clear that a strong lower cut of $E_\gamma > 65$ GeV reduces both the signal and the $\nu\bar{\nu}$ background from the process **(D)**, but does not affect the $\sigma = \frac{S}{\sqrt{B}}$ ratio drastically. The anticipated high luminosity ($\mathcal{L} \sim 10^{33} cm^{-2} sec^{-1} \sim 3 \times 10^4 pb^{-1}$ over a year) [18] ensures that a respectable number of events is obtained in spite of this reduction due to stiff cuts.

Another set of cuts, subjected to a rather strong assumption about the detectors, was discussed in [14]. In particular it was assumed that it is possible to detect in a radiative Bhabha event the scattered e^+ or e^- emitted at an angle $\theta_{min} < \theta_e$ <10° ($\theta_{min} \approx 1.6^\circ$ at $\sqrt{s}$=350 GeV). If this indeed is the case then the above stringent lower p_T cut on the photon can be significantly relaxed. We shall

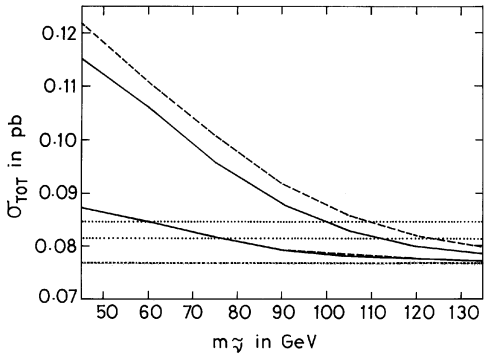

Fig. 6. The total cross section (SM+VLSP) as a function of $m_{\tilde{\nu}}$ at $\sqrt{s}$ =350 GeV. The conventions for different bands and lines are explained in Fig. 3 and in Sect. 3

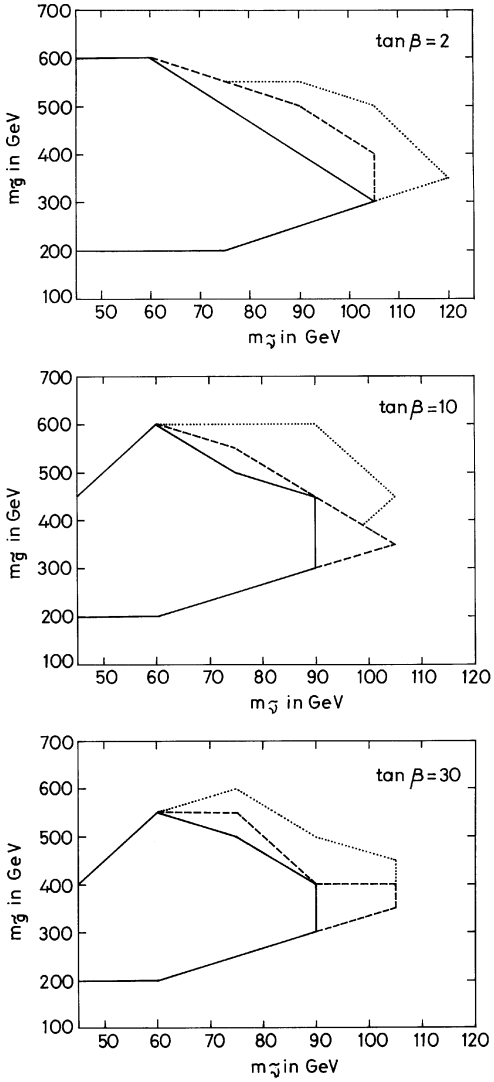

Fig. 7. Contour plots in the $(m_{\tilde{\nu}} - m_{\tilde{g}})$ plane at $\sqrt{s}$ =350 GeV indicating the regions where $\geq 3\sigma$(*dotted*), $\geq 4\sigma$(*dashed*) and $\geq 5\sigma$(*solid*) signals may be obtained for tanβ = 2,10 and 30 and $-500 \leq \mu \leq 500$. We have used $m_{\tilde{g}} \approx 3M_2$ (see Sect. 2)

compare below the effects of these two sets of cuts. It turns out that with the milder cuts of [14] a larger region of the parameter space can be probed.

From Fig. 5b it is clear that the angular distributions for the signal and background processes have similar characteristics. Thus, as in Sect. 2, angular cuts cannot improve the quality of the signal. Nevertheless we impose conservatively angular cuts of $40^\circ < \theta_\gamma < 140^\circ$ which correspond to the central region of the detector where photon detection efficiency is expected to be very high ($\approx$1).

In Fig. 6 we present the cross section as a function of $m_{\tilde{\nu}}$. Throughout this section we use $\mathcal{L} = 3 \times 10^4\,\mathrm{pb}^{-1}$ over a year. The conventions are the same as those in Fig. 3 for the bands and the horizontal lines. The dashed band contains the additional contributions from $\widetilde{N}_1\widetilde{N}_2$ and $\widetilde{N}_2\widetilde{N}_2$ pairs at points where $\widetilde{N}_2$ is also a VLSP. As emphasised in Sect. 2 , the latter contributions will be absent if $m_{\tilde{e}_{L,R}} < \widetilde{N}_2$. As $m_{\tilde{\nu}}$ increases the minimum $m_{\tilde{g}}$ which can accommodate the VLSP scenario also increases (see Fig. 1). For example, at $m_{\tilde{\nu}}$=100 GeV, only $m_{\tilde{g}} \geq$375 GeV are consistent with the VLSP scenario. In addition to the obvious kinematical effects, suppressions due to $\widetilde{\chi}^{\pm}$ and $\tilde{e}_{L,R}$ propagators, therefore, tend to decrease the signal with increasing $m_{\tilde{\nu}}$. Also, for larger $m_{\tilde{g}}$, the contributions from $\widetilde{N}_i\widetilde{N}_j$ pairs decrease due to kinematic effects. The reduction of the total VLSP cross section with increasing $m_{\tilde{\nu}}$ is therefore a complicated combination of several effects. It is clearly seen from Fig. 6 that the SUSY parameter space consistent with the VLSP scenario, indicated by the width of the bands, gradually shrinks as $m_{\tilde{\nu}}$ increases.

We find that for $m_{\tilde{\nu}} \leq$110 GeV a 5σ signal can be obtained even with our conservative cuts without imposing any special requirement on the detectors. This unfortunately is much smaller than the kinematic limit at $\sqrt{s}$=350 GeV. It is therefore worthwhile to study the effects of the relaxed cuts proposed in [14]. We compare the efficiencies of the two sets of cuts in Table 2. The complex interplay between the $m_{\tilde{\nu}}$ and $m_{\tilde{g}}$ in the VLSP scenario, discussed in the last paragraph, is also clearly exhibited in Table 2 which is drawn for $m_{\tilde{g}}$=400 GeV. For this $m_{\tilde{g}}$, the $\widetilde{N}_2$ is not a VLSP for $m_{\tilde{\nu}}$= 110 and 125 GeV, which leads to sleptons lighter than the $\widetilde{N}_2$. The cross section is, therefore, larger for heavier sneutrinos at this $m_{\tilde{g}}$. It follows from this table that significantly larger regions of the parameter space can be scanned if improvement in instrumentation discussed in [14] allows the scattered e^+e^- in a radiative Bhabha event to be tracked down in the beam pipe.

In Fig. 7 we present contour plots in the $(m_{\tilde{g}} - m_{\tilde{\nu}})$ plane that can be probed at $\sqrt{s}$=350 GeV for three values of tanβ, tanβ=2,10,30. In these, the dotted (outermost) contours represent the areas in the $(m_{\tilde{g}} - m_{\tilde{\nu}})$ plane where a $\geq 3\sigma$ signal can be obtained. The dashed (middle ones) and the solid (innermost ones) show the same for 4σ and 5σ signals respectively. As $m_{\tilde{\nu}}$ increases, a distinct rise in the lowest allowed $m_{\tilde{g}}$ is also a very indicative feature of the VLSP scenario.

The photon energy and angular distributions for $\sqrt{s}$ = 500 GeV are shown in Fig. 8a and Fig. 8b respectively.

Table 2. The comparison of the response of the signal to two sets of cuts **A** and **B**[18] at $\sqrt{s}$=350 GeV where Cut **A** $\equiv 65 < E_\gamma < 150$ GeV, $40^\circ < \theta\gamma < 140^\circ$; Cut **B** $\equiv 10 < E_\gamma < 150$ GeV, $10^\circ < \theta\gamma < 170^\circ$, $p_{T_\gamma} > 10$ GeV. Other fixed values of the SUSY parameters used are $(\mu, m_{\tilde{g}}, \tan\beta)$=(−500 GeV, 400 GeV, 2) and $m_{\tilde{e}_L} = m_{\tilde{e}_R}$. The SM background with Cut **A**(**B**) is 0.07671(1.04496)pb. All masses are in GeV and cross-sections are in picobarns. The value of σ corresponds to $\mathcal{L}$ =30 fb^{-1}

$m_{\tilde{\nu}}$	Cut	$\sigma_{\tilde{\nu}\tilde{\nu}}$	$\sigma_{\tilde{N}_1\tilde{N}_1}$	$\sigma_{\tilde{N}_1\tilde{N}_2}$	$\sigma_{\tilde{N}_2\tilde{N}_2}$	Total	$\sigma = \frac{S}{\sqrt{B}}$
110	**A**	.00156	.00212	disallowed$^!$	disallowed$^!$	.00368	2.3
	B	.02037	.01803			.03840	6.7
125	**A**	.00041	.00182	disallowed$^!$	disallowed$^!$	.00223	1.4
	B	.01194	.01600			.02794	4.8
130	**A**	.00018	.00173	.00143	negligible	.00334	2.2
	B	.00948	.01539	.01397	.00101	.03985	6.9
135	**A**	.00004	.00165	.00134	negligible	.00303	1.9
	B	.00721	.01476	.01324	.00096	.03617	6.3
*150	**A**	negligible	.00113	.00074	negligible	.00187	1.2
	B	.00173	.01162	.01060	.00013	.02408	4.1

* In this case $m_{\tilde{g}}$=450 GeV, since $m_{\tilde{g}}$ = 400 GeV is not allowed in the VLSP scenario

$^!$ $\tilde{N}_2$ cannot be a VLSP for this choice of SUSY parameters

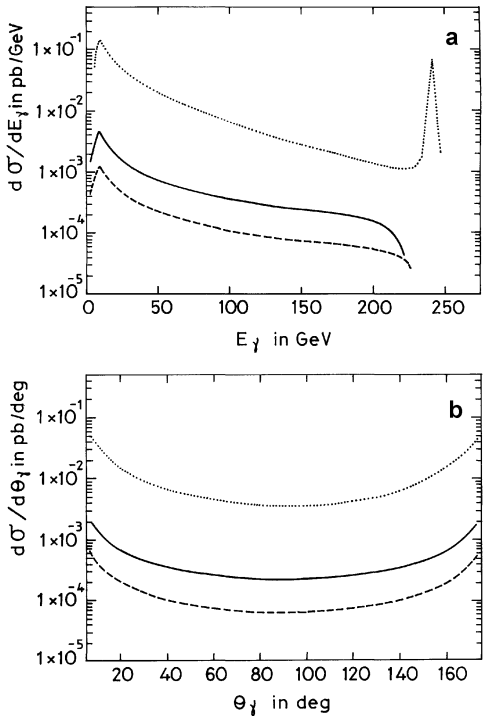

Fig. 8. a Energy distribution of the photon at $\sqrt{s}$ =500 GeV, with $E_\gamma > 5$ GeV and $5^\circ < \theta_\gamma < 175^\circ$. **b** Angular distribution for the photon at $\sqrt{s}$ =500 GeV with $25 < E_\gamma < 225$ and $5^\circ < \theta_\gamma < 175^\circ$. The convention for different lines and SUSY parameters chosen are explained in the text

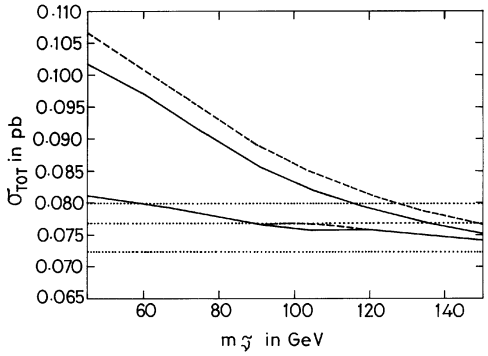

Fig. 9. The total cross section (SM+VLSP) as a function of $m_{\tilde{\nu}}$ at $\sqrt{s}$ =500 GeV. The conventions are the same as in Fig. 6

The conventions and features of the curves are similar to ones for $\sqrt{s}$=350 GeV case. An upper cut of E_γ <225 GeV is set. From kinematical considerations a strong lower cut of $E_\gamma > 95$ GeV is imposed to eliminate completely the radiative Bhabha background. Along with this an angular cut of $40^\circ < \theta\gamma < 140^\circ$ corresponding to the central region of the detector is imposed.

In Fig. 9 we present the cross section as a function of $m_{\tilde{\nu}}$. The conventions are the same as in Fig. 6. We find that only for $m_{\tilde{\nu}} \leq$125 GeV 5σ signals can be obtained using our conservative cuts and optimistic choices of SUSY parameters. It is again much smaller than the kinematic limit at $\sqrt{s}$=500 GeV. Once again by using the relaxed cuts proposed in [14], the search limit can be significantly increased. We compare the efficiencies of the two cuts in Table 3 which shows the prospect of improvement in the search limit if the relaxed cuts [14] are permissible due to improvements in detector designs.

In Fig. 10 we present the contour plots at $\sqrt{s}$=500 GeV for three values of tanβ. The conventions are exactly the same as in Fig. 7.

To end this section it is noteworthy that a greater region in the $(m_{\tilde{\nu}} - m_{\tilde{g}})$ plane can be probed at $\sqrt{s}$=500 GeV with appreciable statistical significance compared to

Table 3. The comparison of the response of the signal to two sets of cuts **A** and **B**[18] at $\sqrt{s}$=500 GeV where Cut **A** $\equiv 95 < E_\gamma < 225$ GeV, $40^\circ < \theta\gamma < 140^\circ$; Cut **B** $\equiv 10 < E_\gamma < 225$ GeV, $10^\circ < \theta\gamma < 170^\circ$, $p_{T_\gamma} > 10$ GeV . Other fixed values of the SUSY parameters used are $(\mu, m_{\tilde{g}}, \tan\beta)$=(−500 GeV, 450 GeV, 2) and $m_{\tilde{e}_L} = m_{\tilde{e}_R}$. The SM background with Cut **A**(**B**) is 0.07227(1.48773)pb. All masses are in GeV and cross-sections are in picobarns. The $S/\sqrt{B}$ ratio corresponds to $\mathcal{L}$ =30 fb^{-1}

$m_{\tilde{\nu}}$	Cut	$\sigma_{\tilde{\nu}\tilde{\nu}}$	$\sigma_{\tilde{N}_1\tilde{N}_1}$	$\sigma_{\tilde{N}_1\tilde{N}_2}$	$\sigma_{\tilde{N}_2\tilde{N}_2}$	Total	$\sigma = \frac{S}{\sqrt{B}}$
150	**A**	.00138	.00156	.00130	.00012	.00436	2.9
	B	.02207	.01417	.01114	.00344	.05082	7.4
155	**A**	.00113	.00150	.00124	.00012	.00399	2.6
	B	.02030	.01378	.01073	.00333	.04814	7.0
† 160	**A**	.00078	.00129	disallowed[!]	disallowed[!]	.00207	1.4
	B	.01582	.01254			.02836	4.1
† 165	**A**	.00060	.00124	.00106	.00004	.00294	1.9
	B	.01430	.01218	.01013	.00231	.03892	5.7
† 170	**A**	.00044	.00120	.00101	.00003	.00268	1.8
	B	.01287	.01185	.00975	.00223	.03670	5.3
‡ 180	**A**	.00017	.00098	.00083	negligible	.00198	1.3
	B	.00852	.01048	.00918	.00136	.02954	4.3

†$m_{\tilde{g}}$=500 GeV

[!] $\widetilde{N}_2$ cannot be a VLSP for this choice of SUSY parameters.

‡$m_{\tilde{g}}$=550 GeV.

the $\sqrt{s}$=350 GeV case, as expected. However, this gain is not commensurate with the increase in beam energy. Also the searches at NLC via this mode will be very effective in constraining the regions of the parameter space which are in principle accessible to direct chargino searches at LEP 2 energies but can not be probed there due to near mass degeneracy of the chargino and the sneutrino and relatively large mass of the sneutrino.

4 The signal in N=1 SUGRA models

In this section we consider a more constrained scenario based on N=1 SUGRA with a common scalar mass (m_0) at the GUT scale [19]. We have taken the usual expressions for the slepton and sneutrino masses including the D term contributions. It should, however, be noted that recently many viable models with non-universal scalar masses have been constructed [20]. Yet models with a common m_0 continue to be popular and its implication for the VLSP scenario is worth investigating. However, no assumption about the Higgs sector and, consequently, about the $SU(2) \otimes U(1)$ breaking mechanism is made. As pointed out in [7] the VLSP scenario can also be accommodated in this more restrictive model. It was shown that the VLSP constraints require a relatively light gluino with $m_{\tilde{g}}$ bounded by the relation

$$m_{1/2} \leq 1.4\sqrt{D_Z}$$

where $m_{1/2}$ is the common gaugino mass at the GUT scale and D_Z has been defined earlier. This bound also restricts the masses of $\widetilde{\chi}_1^\pm$ and $\widetilde{N}_2$ severely. Since in the VLSP scenario the sneutrino has to be lighter than the above particles, $m_{\tilde{\nu}}$ is also bounded from above. As a consequence, this scenario can be tested conclusively at relatively low energy machines, e.g., at an $e^+ e^-$ collider $\sqrt{s}$=350 GeV. Sizable cross sections may be obtained at $\sqrt{s}$=190 GeV provided $m_{\tilde{\nu}}$ happens to be in the lower part of its allowed range.

Here we consider the allowed region of the $(m_0 - m_{1/2})$ mass plane in the VLSP scenario as given in [7]. Using the formulae in [7] one can calculate the sparticle masses and hence the cross sections at various points of the above region using the cuts stated in the earlier sections. We present some of the sample results at $\sqrt{s}$=190 GeV and $\sqrt{s}$=350 GeV in Table 4. It is seen from Table 4 that the entire region of the parameter space allowed in the VLSP scenario gives an observable signal($\geq 5\sigma$) at $\sqrt{s}$=350 GeV. In each case, it turns out that $m_{\tilde{q}}$ is nearly equal to $m_{\tilde{g}}$. Using the bounds of [4] we have restricted ourselves to the cases with $m_{\tilde{q}} = m_{\tilde{g}} \approx 200$ GeV.

If one further assumes radiative breaking of $SU(2) \otimes U(1)$ symmetry then the number of free parameters reduces further. In particular μ becomes a fixed parameter, apart from a sign ambiguity, for given m_0, $m_{1/2}$, $\tan\beta$ and m_t. We have already seen that the cross sections are not very sensitive to μ. We therefore work with the representative choice $\mu = -m_{\tilde{g}}$ used by other authors [21]. The allowed regions of [7] now reduce to narrow strips. In Table 4 we give the cross sections at a few representative points and note that observable signals with high statistical significances are predicted at $\sqrt{s}$=350 GeV.

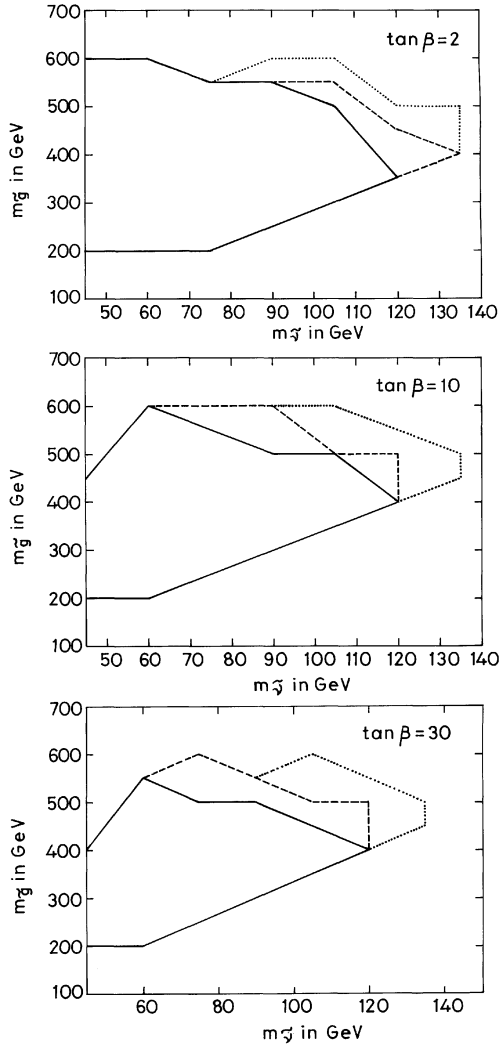

Fig. 10. Contour plots in the $(m_{\tilde{\nu}} - m_{\tilde{g}})$ plane at $\sqrt{s}$ =500 GeV following the conventions of Fig. 7. We have used $m_{\tilde{g}} \approx 3M_2$ (see Sect. 2)

Table 4. Total signal cross section at $\sqrt{s}$ =190 and 350 GeV in N =1 SUGRA model using Cut **A** of Tables 1 and 2. The SUSY parameters consistent with the VLSP scenario are chosen from [7]. The underlined entries correspond to the representative choice $\mu = -m_{\tilde{g}}$ leading to radiative breaking of $SU(2) \otimes U(1)$ symmetry. All masses are in GeV and cross-sections are in picobarns. The values of $\mathcal{L}$ is as in Tables 1 and 2

$\sqrt{s}$	tanβ	m_0	M_2	μ	$m_{\tilde{g}}(m_{\tilde{q}})$	$m_{\tilde{\nu}}$	σ_{SUSY}	$\sigma = \frac{S}{\sqrt{B}}$
hline		20	75	-55	225(225)	47.5	.141	4.7
		40	70	-65	210(213)	53.8	.108	3.6
190	2	30	70	320	210(211)	46.8	.219	7.3
		40	70	400	210(213)	53.8	.170	5.6
		50	70	700	210(215)	61.6	.124	4.1
		50	75	800	225(230)	66.0	.099	3.3
		20	75	-55	225(225)	47.5	.03478	22.3
		40	80	-75	240(242)	63.7	.02338	15.0
		75	70	-125	210(222)	83.2	.01838	11.8
350	2	30	70	320	210(211)	46.8	.05099	32.8
		40	70	500	210(213)	53.8	.04164	26.8
		50	70	1000	210(215)	61.6	.03467	22.3
		55	80	1000	240(245)	74.0	.02494	16.0
		60	70	-160	210(218)	57.6	.121	4.1
		60	70	-210	210(218)	57.6	.118	3.9
		40	80	-120	240(242)	49.7	.144	4.8
190	10	40	90	-120	270(272)	61.5	.094	3.1
		20	90	120	270(270)	50.9	.155	5.1
		60	70	280	210(218)	57.6	.128	4.2
		60	70	500	210(218)	57.6	.121	4.0
		60	70	-210	210(218)	57.6	.03388	21.8
		60	80	-60	240(246)	66.9	.02648	17.0
		60	80	-240	240(246)	66.9	.02605	16.7
		60	90	-200	270(276)	76.1	.02014	12.9
350	10	75	100	-300	300(308)	96.3	.01169	7.5
		40	90	-120	270(272)	61.5	.02789	17.9
		40	90	160	270(272)	61.5	.02990	19.2
		60	100	280	300(305)	85.2	.01292	8.3
		70	85	500	255(263)	80.1	.01960	12.6

5 Radiative corrections

In this section we briefly consider the radiative corrections to the cross sections. We follow the structure function approach of [17]. We, however, restrict ourselves to QED corrections due to soft photon emission to all orders in perturbation theory and lowest order corrections due to single and double hard collinear bremsstrahlung. The formula for the corrected cross section can be found in (5) of the last paper of [17]. In this formula we have substituted the cross sections given in the Appendix. At $\sqrt{s}$ =190 GeV the background increases from 0.45 pb to 0.86 pb with cut A of Table 1. The increase is essentially due to the fact that as a result of the above additional QED corrections, the radiative returns to the Z-pole often occur for E_γ considerably smaller than the tree level value $(s - M_Z^2)/2\sqrt{s}$. Thus the cut E_γ¡ 60 GeV which was devised on the basis of the tree level energy distribution becomes less effective. The changes in the signal cross sections are shown in Table 5. For each sneutrino mass the tree lavel cross sections and that with the radiative corrections are presented using Cut **A** of Table 1. It is seen that the signal reduces marginally due to this correction but the ratio σ (for an integrated luminosity of 500 pb^{-1}) reduces significantly due to increased background.

This exercise shows that whether the $\gamma + \not{E}$ signal will lead to the discovery of SUSY at LEP-2 or will give merely hints for new physics, depends crucially on the correct estimation of the radiative corrections. Thus a more refined analysis including other types of corrections is called for. In particular the following effects should be taken into account: (i) Radiative corrections to the Z-propagator using the usual techniques (see, e.g., the first paper of [17] and references therein). Since radiative returns to the Z-pole is crucially important, these corrections may be non-negligible. (ii) Other QED corrections (see the third Ref. of [17]) like the emission of two overlapping hard photons and radiation of additional hard photons which are not strictly collinear with the beam, but lie within a veto an-

Table 5. Effect of radiative corrections due to soft multiphoton emission and hard collinear bremsstrahlung at LEP-2 energies. For each $m_{\tilde{\nu}}$ the cross sections with and without radiative corrections are presented using the cut **A** of Table 1. The choice of SUSY parameters is $(\mu, m_{\tilde{g}}, \tan\beta)$=(−300 GeV, 200 GeV, 10). All masses are in GeV and cross-sections are in picobarns. The value of $\mathcal{L}$ is as in Table 1

$m_{\tilde{\nu}}$	$\sigma_{\tilde{\nu}\tilde{\nu}}$	$\sigma_{\tilde{N}_1\tilde{N}_1}$	$\sigma_{\tilde{N}_1\tilde{N}_2}$	Total	$\sigma = \frac{S}{\sqrt{B}}$
45	.103	.027	.018	.148	4.9
	.101	.026	.017	.144	3.4
55	.077	.025	.016	.118	3.9
	.069	.024	.015	.108	2.6
65	.048	.023	.015	.086	2.8
	.041	.022	.014	.077	1.8

gle determined by the experimental setup and are lost in the beam pipe.

As has already been discussed, the signal under consideration is of particular interest if the chargino and the sneutrino happen to be nearly mass degenerate. In that case the process $e^+e^- \rightarrow \tilde{\chi}_1^+\tilde{\chi}_1^-\gamma$ followed by the decay $\tilde{\chi}_1^\pm \rightarrow l^\pm\tilde{\nu}$ may also contribute significantly to the signal. This is because the leptons in the final state will be unobservable due to near mass degeneracy of the chargino and the sneutrino. This additional channel is likely to improve the ratio σ compared to the values given in Table 5 in this special case. In fact the radiative chargino pair production has already been discussed in [14], where it was assumed that the charginos decay invisibly due to their near mass degeneracy with the LSP. The tree level calculations of [14] show that a 5σ signal is possible from this channel alone.

6 Conclusions

In our earlier works [2,5–7,23], we had emphasised that currently popular search strategies for supersymmetric particles may be significantly affected in the VLSP scenario. In this scenario relatively light sneutrinos and the second lightest neutralino may decay dominantly into invisible channels, leading to two extra carriers of missing energy (in addition to the lightest supersymmetric particle (LSP)). It is, therefore, worthwhile to identify signals which can distinguish this scenario from the MSSM with conventional mass spectrum.

As an example, we have focussed our attention on the processes (**a**) $e^+e^- \longrightarrow \widetilde{\nu}\widetilde{\bar{\nu}}\gamma$, (**b**) $e^+e^- \longrightarrow \widetilde{N_i}\,\widetilde{N_j}\gamma$ $(i,j$=1,2) both of which contribute to $e^+e^- \longrightarrow \gamma + \not{E}$ in the VLSP scenario. In contrast, only process (**b**) with $i = j$ =1, contributes to the signal in the conventional MSSM. The dominant SM background comes from the process (**c**) $e^+e^- \rightarrow \nu\bar{\nu}\gamma$.

Formulae for the cross sections for the processes (**a-c**), taking into account full mixings of the charginos and the neutralinos are derived and presented in the Appendix. It is found that our estimate of the background agrees with [12] but disagrees with [11] and the last of [17] (for the details see Sect. 2).

Tree level calculations show that for suitable choices of SUSY parameters at LEP-2 energies, process (a) contributes dominantly to the signal. The contribution from $\widetilde{N}_1\,\widetilde{N}_2$ pairs is also comparable to that from LSP pairs, which alone produces the signal in the conventional MSSM. On the other hand, it has already been observed [6,16] that the signal in the conventional MSSM is much below the observable level. This leads to the interesting possibility that at LEP-2 the VLSP scenario can be distinguished not only from the SM but also from the conventional MSSM. After suitable kinematical cuts [6,16], the statistical significance of the signal may be $\geq 5\sigma$ for $45 \leq m_{\tilde{\nu}} \geq 55$GeV and $m_{\tilde{g}} \approx 200$GeV (we have used the approximate relation $m_{\tilde{g}} = 3M_2$ as discussed in Sect. 2).

A preliminary study of a class of radiative corrections, however, shows that the SM background and hence, the statistical significance of the signal depend crucially on them. A more refined analysis taking other similar corrections as suggested in Sect. 5 is, therefore, called for.

It is further shown that a healthy signal is possible for much larger region of the parameter space at a high luminosity e^+e^- collider at 350 and 500 GeV like the proposed NLC machine even with conservative cuts. If further improvements in detector design [14] allow a relaxation of these strong cuts, the VLSP scenario can be distinguished from the conventional MSSM for even larger regions of the parameter space. At $\sqrt{s}$=350(500) GeV, signals with satisfactory statistical significance may be obtained if $m_{\tilde{\nu}} \leq$ 150(180) GeV for $m_{\tilde{g}}$ in the range 400–550 GeV using the cuts of [14]. Another interesting feature is that this signal remains viable even if the mass splitting between the chargino and the sneutrino happens to be small and thus, can play a complementary role to direct chargino searches at LEP-2 and NLC. The latter process can probe larger regions of the parameter space, but the signal may disappear due to the above degeneracy.

The signal remains observable even in the context of more restricted models based on N=1 SUGRA with common scalar and gaugino masses at a high scale.

Appendix

In this appendix we systematically present the relevant formulae for calculating the cross sections of different processes. Throughout this paper we use the following Standard Model Parameters:

$\alpha = 1/128.8$, $G_F = 1.16637 \times 10^{-5}$, $M_Z = 91.187\,GeV$, $M_W = 80.22\,GeV$, $\Gamma_Z = 2.498\,GeV$, $\Gamma_W = 2.25\,GeV$, $T_3^e = -0.5$, $Q_e = -1$, $S_W^2 = sin^2\theta_W = 0.232$, $C_W = cos\theta_W$, $C_V = 2T_3^e - 4Q_eS_W^2$, $C_A = -2T_3^e$, $C_L = C_V - C_A$, $S_{avg} = 1/4$ (spin averaging over the initial spin configuration), $F_{ovl} = 128\pi\alpha G_F^2 M_W^4$.

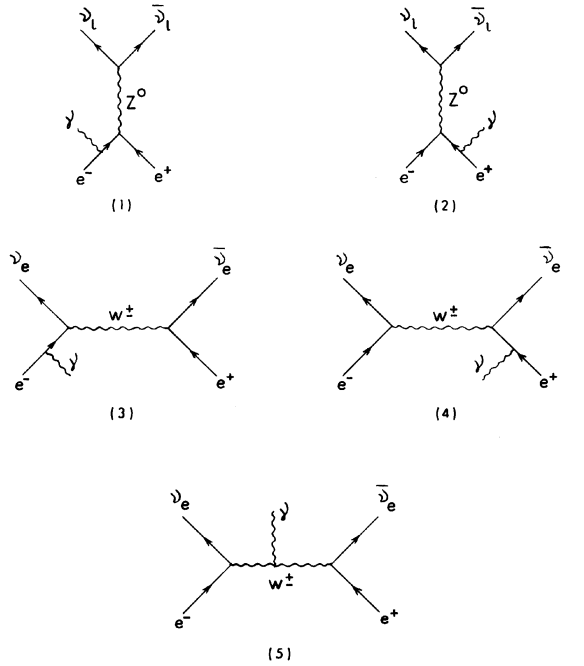

Fig. 11. Feynman diagrams for the process $e^+ e^- \longrightarrow \nu\bar{\nu} + \gamma$. In this and in the subsequent figures, the index l stands for e, μ, τ. Arrows indicate the flow of physical momenta and not of fermion numbers

A: The process $\mathbf{e^+ e^- \longrightarrow \nu\bar{\nu} + \gamma}$

We label the particles by the following indices: $e^+ \Rightarrow 1$, $e^- \Rightarrow 2$, $\nu \Rightarrow 3$, $\bar{\nu} \Rightarrow 4$, $\gamma \Rightarrow 5$. We have used the following abbreviations:
$P_{ij} = p_i.p_j$, $B_W = \frac{1}{(2P_{34}-M_Z^2)^2+(M_Z\Gamma_Z)^2}$, $B = 2P_{34} - M_Z^2$, $W_3 = -(2P_{14} + M_W^2)$, $W_4 = -(2P_{23} + M_W^2)$, $W_{B3} = W_3^2 + (M_W\Gamma_W)^2$, $W_{B4} = W_4^2 + (M_W\Gamma_W)^2$, $\epsilon(ijkl) = \epsilon_{\alpha\beta\gamma\delta}p_i^\alpha p_j^\beta p_k^\gamma p_l^\delta$, where p_i is the momentum of the $i-th$ particle.

In the following $\mathbf{T_{ij}} = A_i A_j^\dagger +$ H.C., where A_i is the amplitude of the $i-th$ Feynman Diagram apart from an overall factor F_{ovl} defined at the begining of this appendix. In this sub-section we consider only the diagrams (Fig. 11) contributing to the cross section of the process $e^+ e^- \longrightarrow \nu\,\bar{\nu} + \gamma$.

The relevant matrix element squared can be computed from the following formulae:

$$\mathbf{T_{11}} = \frac{B_W}{4C_W^4 P_{25}}\Big[(C_V^2 + C_A^2)U_{11} + 2C_V C_A V_{11}\Big],$$
$$\mathbf{U_{11}} = P_{35}(P_{12} - 2P_{13} - P_{15}) + P_{13}(P_{15} + P_{25}) \ ,$$
$$\mathbf{V_{11}} = P_{35}(P_{12} - P_{15}) - P_{13}(P_{15} + P_{25}).$$

$$\mathbf{T_{12}} = \frac{-B_W}{4C_W^4 P_{15}P_{25}}\Big[(C_V^2 + C_A^2)U_{12} + 2C_V C_A V_{12}\Big],$$
$$\mathbf{U_{12}} = -2P_{12}^2(P_{13}+P_{23}-P_{35}) + 2P_{12}P_{13}(P_{15}+2P_{23}+P_{25} - P_{35}) - P_{12}(P_{15}+P_{25})(P_{35}-2P_{23}) + (P_{13}P_{25} - P_{15}P_{23})(2P_{13}+P_{15}-2P_{23}-P_{25}) - 2P_{12}P_{23}P_{35},$$
$$\mathbf{V_{12}} = 2P_{12}^2(P_{13}-P_{23}) - 2P_{12}P_{13}(P_{15}+2P_{25}) + P_{12}P_{15}(4P_{23}-P_{35}) + P_{12}P_{25}(2P_{23}+P_{35}) + (P_{15}+P_{25})(P_{13}P_{25} - P_{15}P_{23}).$$

$$\mathbf{T_{13}} = -\frac{2B_W C_L}{C_W^2 P_{25} W_{B3}}(BW_3 + M_W M_Z \Gamma_W \Gamma_Z) \times\Big[P_{13}(P_{15}+P_{25}-P_{35})\Big].$$

$$\mathbf{T_{14}} = \frac{-B_W C_L}{C_W^2 P_{15}P_{25}W_{B4}}\Big[(BW_4 + M_W M_Z\Gamma_W\Gamma_Z)R_{14} + (M_Z\Gamma_Z W_4 - M_W\Gamma_W B)I_{14}\Big],$$
$$\mathbf{R_{14}} = P_{13}(P_{14}P_{25} - P_{12}P_{45}) - P_{13}P_{24}(P_{15}+P_{25}) - P_{12}P_{24}(P_{35}-2P_{13}) + P_{15}P_{23}P_{24},$$
$$\mathbf{I_{14}} = -\epsilon(3125)P_{24} + \epsilon(4125)P_{13}.$$

$$\mathbf{T_{15}} = \frac{B_W C_L}{C_W^2 P_{25} W_{B3} W_{B4}}\Big[\Big\{B(W_3W_4 - M_W^2\Gamma_W^2) + M_Z M_W \Gamma_Z\Gamma_W(W_3+W_4)\Big\}R_{15} - \Big\{B(W_3+W_4)M_W\Gamma_W - M_Z\Gamma_Z(W_3W_4 - M_W^2\Gamma_W^2)\Big\}I_{15}\Big],$$
$$\mathbf{R_{15}} = (3P_{24}-P_{45})(P_{15}P_{23} - P_{12}P_{35}) - P_{13}P_{24}(P_{15} - 2P_{23} + 2P_{24} + 2P_{25} - 2P_{45} - 2P_{12}) + P_{14}P_{25}(P_{13}-P_{23}) - P_{13}P_{45}(P_{12} - 3P_{25} + 2P_{23}) + P_{12}P_{25}P_{34},$$
$$\mathbf{I_{15}} = -\epsilon(3425)\Big[P_{12}+P_{15}\Big] + \epsilon(4125)\Big[P_{13}-P_{23}-P_{35}\Big] - 2\epsilon(3125)(P_{24}-P_{45}) + \epsilon(3415)P_{25}$$

$$\mathbf{T_{22}} = \frac{B_W}{4C_W^4 P_{15}}\Big[(C_V^2 + C_A^2)U_{22} + 2C_V C_A V_{22}\Big],$$
$$\mathbf{U_{22}} = (P_{12} - 2P_{23} - P_{25})P_{35} + (P_{15}+P_{25})P_{23},$$
$$\mathbf{V_{22}} = (P_{25} - P_{12})P_{35} + (P_{15}+P_{25})P_{23}.$$

$$\mathbf{T_{23}} = \frac{-B_W C_L}{C_W^2 P_{15}P_{25}W_{B3}}\Big[(BW_3 + M_W M_Z\Gamma_W\Gamma_Z)R_{23} + (M_Z\Gamma_Z W_3 - M_W\Gamma_W B)I_{23}\Big],$$
$$\mathbf{R_{23}} = P_{13}P_{25}(P_{14}-P_{24}) - P_{15}P_{24}(P_{13}-P_{23}) + P_{12}P_{24}(2P_{13}-P_{35}) - P_{12}P_{13}P_{45},$$
$$\mathbf{I_{23}} = \epsilon(3125)P_{24} - \epsilon(4125)P_{13}.$$

$$\mathbf{T_{24}} = \frac{-2B_W C_L}{C_W^2 P_{15} W_{B4}} \times(BW_4 + M_W M_Z\Gamma_W\Gamma_Z)\Big[P_{35}(P_{12}-P_{23}-P_{25})\Big].$$

$$\mathbf{T_{25}} = \frac{-B_W C_L}{C_W^2 P_{15} W_{B3} W_{B4}} \Big[\Big\{ B(W_3 W_4 - M_W^2 \Gamma_W^2) + M_Z M_W \Gamma_Z \Gamma_W (W_3 + W_4) \Big\} R_{25} - \Big\{ B(W_3 + W_4) M_W \Gamma_W - M_Z \Gamma_Z (W_3 W_4 - M_W^2 \Gamma_W^2) \Big\} I_{25} \Big],$$

$$\mathbf{R_{25}} = -P_{12}P_{13}(P_{34} - P_{45}) - P_{12}P_{35}(P_{24} - P_{34} - P_{45}) + P_{13}P_{14}(P_{23} - 2P_{24} - P_{25}) + P_{13}P_{24}(P_{13} + P_{15} + P_{25} - P_{35} + P_{45}) - P_{14}P_{35}(P_{23} - P_{24} + P_{25}) - P_{15}P_{24}(P_{23} + P_{34} + 3P_{35}),$$

$$\mathbf{I_{25}} = \epsilon(3415)(P_{13} + P_{24}) + \epsilon(4125)(P_{13} + P_{35}) - \epsilon(3125)P_{24} - \epsilon(3412)P_{35}.$$

$$\mathbf{T_{33}} = \frac{4}{P_{25} W_{B3}} \Big[P_{13}(P_{15} + P_{25} - P_{35}) \Big].$$

$$\mathbf{T_{34}} = \frac{4}{P_{15} P_{25} W_{B3} W_{B4}} \Big[(W_3 W_4 + M_W^2 \Gamma_W^2) R_{34} - M_W \Gamma_W (W_3 - W_4) I_{34} \Big],$$

$$\mathbf{R_{34}} = P_{12}P_{13}(2P_{12} - 2P_{15} - 2P_{23} - 3P_{25} + P_{35}) - P_{12}P_{35}(P_{12} - P_{23} - P_{25}) - (P_{13} - P_{23} - P_{25})(P_{13}P_{25} - P_{15}P_{23}) + P_{12}P_{15}P_{23},$$

$$\mathbf{I_{34}} = -\epsilon(3125)(P_{12} + P_{13} - P_{23} - P_{25}).$$

$$\mathbf{T_{35}} = \frac{-4}{P_{25} W_{B3} W_{B4}} \Big[W_4 R_{35} - M_W \Gamma_W I_{35} \Big],$$

$$\mathbf{R_{35}} = -P_{12}P_{35}(3P_{12} + P_{13} - P_{15} - 3P_{23} - 3P_{25} + P_{35}) + P_{12}P_{13}(4P_{23} + P_{25}) + P_{15}P_{23}(3P_{12} - 3P_{13} - P_{15} - 3P_{23} - 3P_{25} + P_{35}) + P_{13}P_{25}(P_{13} + 3P_{15} - 5P_{23} + 3P_{25} - 3P_{35}) - 4P_{13}P_{23}(P_{23} - P_{35}),$$

$$\mathbf{I_{35}} = -(3P_{12} + P_{13} - P_{15} - 3P_{23} - 3P_{25} + P_{35}).\epsilon(3125)$$

$$\mathbf{T_{44}} = \frac{4}{P_{15} W_{B4}} \Big[P_{35}(P_{12} - P_{23} - P_{25}) \Big].$$

$$\mathbf{T_{45}} = \frac{8}{P_{15} W_{B3} W_{B4}} \Big[W_3 R_{45} - M_W \Gamma_W I_{45} \Big],$$

$$\mathbf{R_{45}} = -P_{12}P_{13}(P_{12} - P_{13} - 2P_{15} - P_{23} - 2P_{25} + P_{35}) - P_{12}P_{15}(P_{23} + P_{35}) - P_{13}P_{23}(2P_{13} + 2P_{15} + P_{25} - 2P_{35}) - P_{13}P_{25}(P_{13} + P_{15} + P_{25} - 2P_{35}) + P_{15}P_{23}(P_{23} + P_{25} + 2P_{35}) - P_{35}(P_{12}P_{35} - 2P_{15}P_{25}),$$

$$\mathbf{I_{45}} = -(P_{12} + P_{13} - P_{23} - P_{25})\epsilon(3125).$$

$$\mathbf{T_{55}} = \frac{-4}{W_{B3} W_{B4}} \Big[U_{55} \Big],$$

$$\mathbf{U_{55}} = -P_{12}P_{23}(P_{12} + 6P_{13} + 5P_{15} - P_{23} - P_{25} + 4P_{35}) + P_{12}P_{35}(3P_{12} + P_{13} - 3P_{15} - 3P_{25} - P_{35}) - P_{13}P_{25}(P_{12} + 3P_{13} + 3P_{15} - 8P_{23} + 3P_{25} - 7P_{35}) - P_{13}P_{23}(P_{13} - 5P_{15} - 7P_{23} + 3P_{35}) + 2P_{15}P_{23}(P_{15} + 3P_{23} + 3P_{25} + P_{35}) + 4P_{15}P_{25}P_{35}.$$

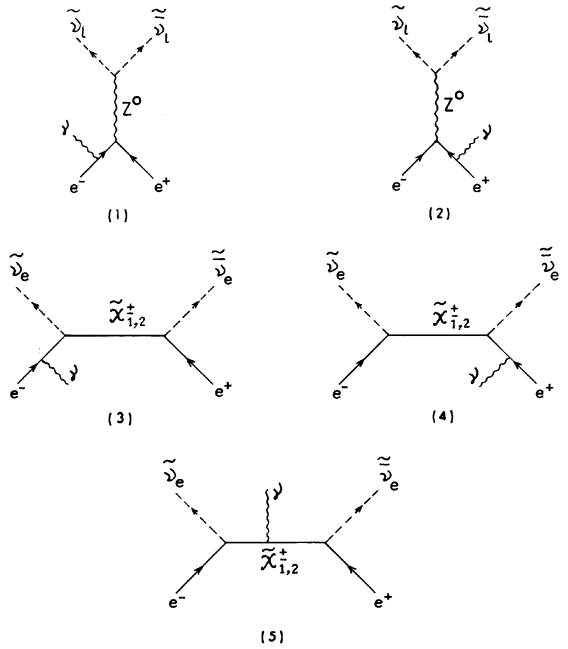

Fig. 12. Feynman diagrams for the process $e^+ e^- \longrightarrow \tilde{\nu}\bar{\tilde{\nu}} + \gamma$

$$T(\nu\bar{\nu}) = 3(T_{11} + T_{12} + T_{22}) + T_{13} + T_{14} + T_{15} + T_{23} + T_{24} + T_{25} + T_{33} + T_{34} + T_{35} + T_{44} + T_{45} + T_{55}$$

The differential cross section is given by

$$d\sigma = F_{ovl} S_{avg} \frac{T(\nu\bar{\nu})}{64 E_{CM}^2 \pi^5} \delta^4 \Big(p_1 + p_2 - \sum_{i=3}^{5} p_i \Big) \prod_{i=3}^{5} \frac{d^3 p_i}{2E_i}$$

Other cross sections are obtained by replacing the T-factor in the above formula by the appropriate expressions calculated in the following appendices.

B: The process e$^+$ e$^-$ $\longrightarrow \tilde{\nu}\bar{\tilde{\nu}} + \gamma$

In this subsection we consider the diagrams (Fig. 12) contributing to the cross section of the process $e^+e^- \longrightarrow \tilde{\nu}\bar{\tilde{\nu}} + \gamma$. We define for this subsection:

$$B_W = \frac{1}{\Big\{ 2(m_{\tilde{\nu}}^2 + P_{34}) - M_Z^2 \Big\}^2 + (M_Z \Gamma_Z)^2}.$$

We label the particles by the following indices: $\tilde{\nu} \Rightarrow 3, \bar{\tilde{\nu}} \Rightarrow 4$, while the indices 1, 2 and 5 have the same meanining as in the previous subsection.

The convention for the T_{ij}-s in this subsection is the same as in the last subsection for the process under consideration.

$$\mathbf{T_{11}} = \frac{3B_W}{8C_W^4 P_{25}} (C_V^2 + C_A^2) \Big[(P_{13} - P_{14})(P_{35} - P_{45}) + P_{15}(P_{34} - m_{\tilde{\nu}}^2) \Big].$$

$$\mathbf{T_{12}} = \frac{-3B_W}{8C_W^4 P_{15}P_{25}}(C_V^2+C_A^2)U_{12},$$
$$\mathbf{U_{12}} = P_{12}\Big\{2(P_{12}-P_{15}-P_{25})(m_{\tilde\nu}^2-P_{34})-(P_{13}-P_{14})(2P_{23}-2P_{24}-P_{35}+P_{45})+(P_{23}-P_{24})(P_{35}-P_{45})\Big\}+P_{15}\Big\{P_{23}(P_{13}-P_{14}-P_{23}+2P_{24})-P_{24}(P_{13}-P_{14}+P_{24})\}-P_{25}\{P_{13}(P_{13}-2P_{14}-P_{23}+P_{24})+P_{14}(P_{14}+P_{23}-P_{24})\Big\}.$$

$$\mathbf{T_{13}} = -\frac{B_W C_L}{2C_W^2 P_{25}}(M_Z^2-2m_{\tilde\nu}^2-2P_{34})\sum_{a=1}^{2}\frac{|\mathcal{V}_{a1}|^2}{(m_{\tilde\nu}^2-m_a^2-2P_{14})}\Big[U_{13}\Big],$$
$$\mathbf{U_{13}} = -P_{12}(2P_{25}-3P_{35})+P_{13}(3P_{25}-4P_{35})+P_{15}(2m_{\tilde\nu}^2-3P_{23})$$

where $\mathcal{V}_{a1}$, a=1,2 are the mixing factors corresponding to the lighter and heavier chargino respectively and m_a, a =1,2 are the masses of these charginos.

$$\mathbf{T_{14}} = -\frac{B_W C_L}{2C_W^2 P_{15}P_{25}}(M_Z^2-2m_{\tilde\nu}^2-2P_{34})\sum_{a=1}^{2}\frac{|\mathcal{V}_{a1}|^2}{(m_{\tilde\nu}^2-m_a^2-2P_{23})}\Big[U_{14}\Big],$$
$$\mathbf{U_{14}} = 2(m_{\tilde\nu}^2P_{12}-P_{13}P_{23})(P_{12}-P_{15}-P_{25})+P_{12}P_{35}(2P_{13}+2P_{23}-P_{25})-P_{13}P_{25}(2P_{13}-P_{25})-P_{15}P_{23}(2P_{23}+P_{25})-2P_{12}P_{13}P_{23}.$$

$$\mathbf{T_{15}} = -\frac{B_W C_L}{C_W^2 P_{25}}(M_Z^2-2m_{\tilde\nu}^2-2P_{34})\sum_{a=1}^{2}\frac{|\mathcal{V}_{a1}|^2}{(m_{\tilde\nu}^2-m_a^2-2P_{14})(m_{\tilde\nu}^2-m_a^2-2P_{23})}\times\Big[2U_{15}-m_a^2W_{15}\Big],$$
$$\mathbf{U_{15}} = P_{23}\Big\{m_{\tilde\nu}^2(P_{15}-P_{12})-P_{25}(P_{12}-3P_{13}-P_{15})+2P_{13}(P_{23}-P_{35})\Big\},$$
$$\mathbf{W_{15}} = P_{12}(P_{25}-P_{35})-P_{13}P_{25}+P_{15}P_{23}.$$

$$\mathbf{T_{22}} = \frac{3B_W}{4C_W^4 P_{15}}(C_V^2+C_A^2)\Big[(P_{23}-P_{24})(P_{35}-P_{45})+P_{25}(P_{34}-m_{\tilde\nu}^2)\Big].$$

$$\mathbf{T_{23}} = -\frac{-B_W C_L}{2C_W^2 P_{15}P_{25}}(M_Z^2-2m_{\tilde\nu}^2-2P_{34})\sum_{a=1}^{2}\frac{|\mathcal{V}_{a1}|^2}{(m_{\tilde\nu}^2-m_a^2-2P_{14})}\Big[U_{23}\Big],$$
$$\mathbf{U_{23}} = -P_{12}\Big\{2m_{\tilde\nu}^2(P_{12}-P_{15}-P_{25})-2P_{13}(2P_{23}-P_{35})+P_{15}(2P_{25}-P_{35})+2P_{35}(P_{23}-P_{25})\Big\}+(P_{13}P_{25}-P_{15}P_{23})(2P_{13}+P_{15}-2P_{23}-2P_{25}).$$

$$\mathbf{T_{24}} = \frac{B_W C_L}{2C_W^2 P_{15}}(M_Z^2-2m_{\tilde\nu}^2-2P_{34})\sum_{a=1}^{2}\frac{|\mathcal{V}_{a1}|^2}{(m_{\tilde\nu}^2-m_a^2-2P_{23})}\Big[U_{24}\Big],$$
$$\mathbf{U_{24}} = P_{25}(P_{13}-2m_{\tilde\nu}^2)-P_{35}(P_{12}-4P_{23})-P_{15}P_{23}.$$

$$\mathbf{T_{25}} = \frac{B_W C_L}{C_W^2 P_{15}}(M_Z^2-2m_{\tilde\nu}^2-2P_{34})\sum_{a=1}^{2}\frac{|\mathcal{V}_{a1}|^2}{(m_{\tilde\nu}^2-m_a^2-2P_{14})(m_{\tilde\nu}^2-m_a^2-2P_{23})}\times\Big[2U_{25}-m_a^2W_{25}\Big],$$
$$\mathbf{U_{25}} = m_{\tilde\nu}^2\Big\{P_{12}(P_{12}-P_{13}-P_{15}-P_{25})+P_{25}(P_{13}+P_{15})\Big\}-P_{23}(2P_{13}+P_{15}-2P_{35})\times(P_{12}-P_{13}-P_{15}),$$
$$\mathbf{W_{25}} = P_{12}(P_{15}-P_{35})+P_{13}P_{25}-P_{15}P_{23}.$$

$$\mathbf{T_{33}} = \frac{4}{P_{25}}\sum_{a=1}^{2}\sum_{b=1}^{2}\frac{|\mathcal{V}_{a1}|^2|\mathcal{V}_{b1}|^2}{(m_{\tilde\nu}^2-m_a^2-2P_{14})(m_{\tilde\nu}^2-m_b^2-2P_{14})}\times\Big[2P_{14}P_{45}-m_{\tilde\nu}^2P_{15}\Big].$$

$$\mathbf{T_{34}} = \frac{4}{P_{15}P_{25}}\sum_{a=1}^{2}\sum_{b=1}^{2}\frac{|\mathcal{V}_{a1}|^2|\mathcal{V}_{b1}|^2}{(m_{\tilde\nu}^2-m_a^2-2P_{14})(m_{\tilde\nu}^2-m_b^2-2P_{23})}\Big[U_{34}\Big],$$
$$\mathbf{U_{34}} = P_{12}\Big\{-m_{\tilde\nu}^2(P_{12}-P_{15}-P_{25})+P_{13}(2P_{23}-P_{35})-P_{35}(P_{23}-P_{25})\Big\}+(P_{13}P_{25}-P_{15}P_{23})(P_{13}-P_{23}-P_{25}).$$

$$\mathbf{T_{35}} = \frac{4}{P_{25}}\sum_{a=1}^{2}\sum_{b=1}^{2}\frac{|\mathcal{V}_{a1}|^2|\mathcal{V}_{b1}|^2}{(m_{\tilde\nu}^2-m_a^2-2P_{14})(m_{\tilde\nu}^2-m_b^2-2P_{14})(m_{\tilde\nu}^2-m_b^2-2P_{23})}\times\Big[2U_{35}-m_b^2W_{35}\Big],$$
$$\mathbf{U_{35}} = P_{23}\Big\{m_{\tilde\nu}^2(P_{12}-P_{15})-2P_{14}(P_{24}-P_{45})\Big\},$$
$$\mathbf{W_{35}} = -P_{12}P_{45}-P_{14}P_{25}+P_{15}P_{24}.$$

$$\mathbf{T_{44}} = \frac{4}{P_{15}} \sum_{a=1}^{2} \sum_{b=1}^{2} \frac{|\mathcal{V}_{a1}|^2 |\mathcal{V}_{b1}|^2}{(m_{\tilde{\nu}}^2 - m_a^2 - 2P_{23})(m_{\tilde{\nu}}^2 - m_b^2 - 2P_{23})} \times \Big[2P_{23}P_{35} - m_{\tilde{\nu}}^2 P_{25}\Big] .$$

$$\mathbf{T_{45}} = \frac{4}{P_{15}} \sum_{a=1}^{2} \sum_{b=1}^{2} \frac{|\mathcal{V}_{a1}|^2 |\mathcal{V}_{b1}|^2}{(m_{\tilde{\nu}}^2 - m_a^2 - 2P_{23})(m_{\tilde{\nu}}^2 - m_b^2 - 2P_{23})(m_{\tilde{\nu}}^2 - m_b^2 - 2P_{14})} \times \Big[2U_{45} - m_b^2 W_{45}\Big] ,$$

$$\mathbf{U_{45}} = m_{\tilde{\nu}}^2 \Big\{ P_{12}(P_{12} - P_{13} - P_{15} - P_{25}) + P_{25}(P_{13} + P_{15}) \Big\} - 2P_{13}P_{23}(P_{12} - P_{13} - P_{15} + P_{35}) + 2P_{23}P_{35}(P_{12} - P_{15}),$$

$$\mathbf{W_{45}} = -P_{12}P_{35} + P_{13}P_{25} - P_{15}P_{23}.$$

$$\mathbf{T_{55}} = \frac{8}{P_{15}} \sum_{a=1}^{2} \sum_{b=1}^{2} \frac{|\mathcal{V}_{a1}|^2 |\mathcal{V}_{b1}|^2 \Big[U_{55} - 2(m_a^2 + m_b^2) W_{55} + m_a^2 m_b^2 P_{12}\Big]}{(m_{\tilde{\nu}}^2 - m_a^2 - 2P_{14})(m_{\tilde{\nu}}^2 - m_a^2 - 2P_{23})(m_{\tilde{\nu}}^2 - m_b^2 - 2P_{14})(m_{\tilde{\nu}}^2 - m_b^2 - 2P_{23})},$$

$$\mathbf{U_{55}} = m_{\tilde{\nu}}^2 \Big\{ P_{12}(m_{\tilde{\nu}}^2 - 4P_{23} + 2P_{35}) - 2P_{13}P_{25} + 2P_{15}(P_{23} - P_{25}) \Big\} + 4P_{23}(P_{23} - P_{35})(P_{12} - P_{15}) + 4P_{13}P_{23}P_{25},$$

$$\mathbf{W_{55}} = P_{23}(-P_{12} + P_{13} + P_{15}).$$

$$T(\tilde{\nu}\bar{\tilde{\nu}}) = \sum_{\substack{i,j=1 \\ j \geq 1}}^{5} T_{ij}$$

C: The process $\mathbf{e^+ e^- \longrightarrow \widetilde{N}_i \widetilde{N}_j + \gamma}$

In this subsection we give the formula for the cross section of the process $e^+e^- \longrightarrow \widetilde{N}_i\widetilde{N}_j + \gamma$. The contributing Feynman diagrams are as in Fig. 13. We define for this subsection:

$$S = m_i^2 + m_j^2 + 2P_{34} - M_Z^2$$

$$B_W = \frac{1}{(m_i^2 + m_j^2 + 2P_{34} - M_Z^2)^2 + M_Z^2\Gamma_Z^2}$$

In this subsection we label the particles by the following indices: 3 and 4 stand for $\widetilde{N}_i$ and $\widetilde{N}_j$ respectively where i,j=1,2 and $i \leq j$. The labels 1,2,5 have the same meaning as in the previous subsection. In the following the formulae for the t-channel selectron exchange diagrams (diagrams 3 to 8 in Fig. 13) are given in terms of $\tilde{l}_h$ ($h = L, R$). The summation over two scalar degrees of freedom is expicitely carried out in the last step where $T(\widetilde{N}_i\widetilde{N}_j)$ is calculated.

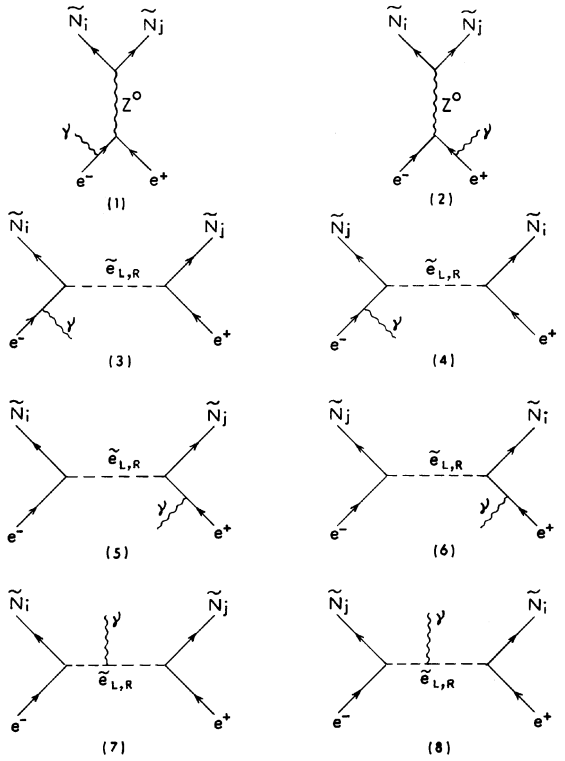

Fig. 13. Feynman diagrams for the process $e^+ e^- \longrightarrow \widetilde{N}_i\widetilde{N}_j + \gamma$

The convention for the T_{ij}-s in this subsection is the same as in the last subsection for the process under consideration.

$$\mathbf{T_{11}} = -\frac{(C_A^2 + C_V^2)G_A^2}{2P_{25}} \Big[m_i m_j P_{15} - P_{14}P_{35} - P_{13}P_{45}\Big]$$

$$\mathbf{T_{12}} = -\frac{(C_A^2 + C_V^2)G_A^2}{2P_{15}P_{25}} \Big[(P_{12} - P_{15} - P_{25})(2m_i m_j P_{12} - P_{13}P_{24} - P_{14}P_{23}) - P_{12}\Big\{P_{13}P_{24} + P_{14}P_{23} - P_{35}(P_{14} + P_{24}) - P_{45}(P_{13} + P_{23})\Big\} - 2(P_{15}P_{23}P_{24} + P_{13}P_{14}P_{25})\Big]$$

$$\mathbf{T_{13}} = -\frac{2C_L G_A}{P_{25}(m_j^2 - 2P_{14} - m_{\tilde{e}_h}^2)} \Big[m_i m_j P_{15} - 2P_{14}P_{35}\Big]$$

$$\mathbf{T_{14}} = -\mathbf{T_{13}} \left\{ \begin{matrix} i \leftrightarrow j \\ 3 \leftrightarrow 4 \end{matrix} \right\}$$

$$\mathbf{T_{15}} = \frac{2C_L G_A}{P_{15}P_{25}(m_i^2 - 2P_{23} - m_{\tilde{e}_h}^2)} \Big[(P_{12} - P_{15} - P_{25})(m_i m_j P_{12} - P_{14}P_{23}) - P_{23}(P_{12}P_{14} + P_{15}P_{24} - P_{12}P_{45}) - P_{14}(P_{13}P_{25} - P_{12}P_{35})\Big]$$

$$\mathbf{T_{16}} = -\mathbf{T_{15}} \left\{ \begin{array}{l} i \leftrightarrow j \\ 3 \leftrightarrow 4 \end{array} \right\}$$

$$\begin{aligned}\mathbf{T_{17}} = & \frac{C_L G_A}{P_{25}(m_i^2 - 2P_{23} - m_{\tilde{e}_h}^2)(m_j^2 - 2P_{14} - m_{\tilde{e}_h}^2)} \\ & \times \Big[m_i m_j \Big\{ P_{12}(-2P_{12} + 2P_{15} - 2P_{23} + 2P_{24} + P_{35} - P_{45}) \\ & + P_{15}(P_{23} - P_{24}) - P_{25}(P_{13} - P_{14}) \Big\} \\ & + 2P_{14} \Big\{ P_{23}(2P_{12} - P_{15} + 2P_{23} - 2P_{24} - 2P_{35} + P_{45}) \\ & + P_{25}(m_i^2 + P_{13} - P_{34}) - P_{35}(P_{12} - P_{24}) \Big\} \Big]\end{aligned}$$

$$\mathbf{T_{18}} = -\mathbf{T_{17}} \left\{ \begin{array}{l} i \leftrightarrow j \\ 3 \leftrightarrow 4 \end{array} \right\}$$

$$\mathbf{T_{22}} = \mathbf{T_{11}}(1 \leftrightarrow 2)$$

$$\begin{aligned}\mathbf{T_{23}} = & \frac{2C_L G_A}{P_{15} P_{25}(m_i^2 - 2P_{14} - m_{\tilde{e}_h}^2)} \\ & \times \Big[(P_{12} - P_{15} - P_{25})(m_i m_j P_{12} - P_{14} P_{23}) \\ & - P_{23}(P_{12} P_{14} - P_{12} P_{45} + P_{15} P_{24}) - P_{14}(P_{13} P_{25} - P_{12} P_{35}) \Big]\end{aligned}$$

$$\mathbf{T_{24}} = -\mathbf{T_{23}} \left\{ \begin{array}{l} i \leftrightarrow j \\ 3 \leftrightarrow 4 \end{array} \right\}$$

$$\mathbf{T_{25}} = \frac{2C_L G_A}{P_{15}(m_i^2 - 2P_{23} - m_{\tilde{e}_h}^2)} \Big[m_i m_j P_{25} - 2P_{23} P_{45} \Big]$$

$$\mathbf{T_{26}} = -\mathbf{T_{25}} \left\{ \begin{array}{l} i \leftrightarrow j \\ 3 \leftrightarrow 4 \end{array} \right\}$$

$$\begin{aligned}\mathbf{T_{27}} = & \frac{C_L G_A}{P_{15}(m_i^2 - 2P_{23} - m_{\tilde{e}_h}^2)(m_j^2 - 2P_{14} - m_{\tilde{e}_h}^2)} \\ & \times \Big[m_i m_j \Big\{ P_{12}(-2P_{12} + 2P_{13} - 2P_{14} + 2P_{25} - P_{35} + P_{45}) \\ & + P_{15}(P_{23} - 2P_{24}) - P_{25}(P_{13} - P_{14}) \Big\} \\ & + 2P_{23} \Big\{ P_{14}(2P_{12} - 2P_{13} + 2P_{14} - P_{25} + P_{35} - 2P_{45}) \\ & + P_{15}(m_j^2 + P_{24} - P_{34}) - P_{45}(P_{12} - P_{13}) \Big\} \Big]\end{aligned}$$

$$\mathbf{T_{28}} = -\mathbf{T_{27}} \left\{ \begin{array}{l} i \leftrightarrow j \\ 3 \leftrightarrow 4 \end{array} \right\}$$

$$\mathbf{T_{33}} = \frac{16 P_{14} P_{35}}{P_{25}(m_j^2 - 2P_{14} - m_{\tilde{e}_h}^2)^2}$$

$$\mathbf{T_{34}} = \frac{16 m_i m_j P_{15}}{P_{25}(m_i^2 - 2P_{13} - m_{\tilde{e}_h}^2)(m_j^2 - 2P_{14} - m_{\tilde{e}_h}^2)}$$

$$\begin{aligned}\mathbf{T_{35}} = & \frac{16}{P_{15} P_{25}(m_i^2 - 2P_{23} - m_{\tilde{e}_h}^2)(m_j^2 - 2P_{14} - m_{\tilde{e}_h}^2)} \\ & \times \Big[P_{14} P_{23}(2P_{12} - P_{15} - P_{25}) + P_{14}(P_{13} P_{25} - P_{12} P_{35}) \\ & + P_{23}(P_{15} P_{24} - P_{12} P_{45}) \Big]\end{aligned}$$

$$\begin{aligned}\mathbf{T_{36}} = & \frac{16 m_i m_j P_{12}(P_{12} - P_{15} - P_{25})}{P_{15} P_{25}(m_j^2 - 2P_{24} - m_{\tilde{e}_h}^2)(m_j^2 - 2P_{14} - m_{\tilde{e}_h}^2)}\end{aligned}$$

$$\begin{aligned}\mathbf{T_{37}} = & \frac{-16 P_{14}}{P_{25}(m_i^2 - 2P_{23} - m_{\tilde{e}_h}^2)(m_j^2 - 2P_{14} - m_{\tilde{e}_h}^2)^2} \\ & \times \Big[P_{23}(2P_{12} - P_{15} + 2P_{23} - 2P_{24} - 2P_{35} + P_{45}) \\ & + P_{25}(m_i^2 + P_{13} - P_{34}) - P_{35}(P_{12} - P_{24}) \Big]\end{aligned}$$

$$\begin{aligned}\mathbf{T_{38}} = & \\ & \frac{-8 m_i m_j}{P_{25}(m_i^2 - 2P_{13} - m_{\tilde{e}_h}^2)(m_j^2 - 2P_{14} - m_{\tilde{e}_h}^2)(m_j^2 - 2P_{24} - m_{\tilde{e}_h}^2)} \\ & \Big[P_{12}(2P_{12} - 2P_{15} - 2P_{23} + 2P_{24} + P_{35} - P_{45}) \\ & + P_{15}(P_{23} - P_{24}) - P_{25}(P_{13} - P_{14}) \Big]\end{aligned}$$

$$\mathbf{T_{44}} = \mathbf{T_{33}} \left\{ \begin{array}{l} i \leftrightarrow j \\ 3 \leftrightarrow 4 \end{array} \right\}$$

$$\mathbf{T_{45}} = \mathbf{T_{36}} \left\{ \begin{array}{l} i \leftrightarrow j \\ 3 \leftrightarrow 4 \end{array} \right\}$$

$$\mathbf{T_{46}} = \mathbf{T_{35}} \left\{ \begin{array}{l} i \leftrightarrow j \\ 3 \leftrightarrow 4 \end{array} \right\}$$

$$\mathbf{T_{47}} = \mathbf{T_{38}} \left\{ \begin{array}{l} i \leftrightarrow j \\ 3 \leftrightarrow 4 \end{array} \right\}$$

$$\mathbf{T_{48}} = \mathbf{T_{37}} \left\{ \begin{array}{l} i \leftrightarrow j \\ 3 \leftrightarrow 4 \end{array} \right\}$$

$$\mathbf{T_{55}} = \frac{16 P_{23} P_{45}}{P_{15}(m_i^2 - 2P_{23} - m_{\tilde{e}_h}^2)^2}$$

$$\mathbf{T_{56}} = \frac{16 m_i m_j P_{25}}{P_{15}(m_i^2 - 2P_{23} - m_{\tilde{e}_h}^2)(m_j^2 - 2P_{24} - m_{\tilde{e}_h}^2)}$$

$$\begin{aligned}\mathbf{T_{57}} = & \frac{-16 P_{23}}{P_{15}(m_i^2 - 2P_{23} - m_{\tilde{e}_h}^2)^2(m_j^2 - 2P_{14} - m_{\tilde{e}_h}^2)} \\ & \times \Big[(P_{12} - P_{13} + P_{14})(2P_{14} - P_{45}) - P_{14}(P_{25} - P_{35} + P_{45}) \\ & + P_{15}(m_j^2 + P_{24} - P_{34}) \Big]\end{aligned}$$

$$\begin{aligned}\mathbf{T_{58}} = & \\ & \frac{-8 m_i m_j}{P_{15}(m_i^2 - 2P_{13} - m_{\tilde{e}_h}^2)(m_i^2 - 2P_{23} - m_{\tilde{e}_h}^2)(m_j^2 - 2P_{24} - m_{\tilde{e}_h}^2)} \\ & \times \Big[(P_{13} - P_{14})(2P_{12} - P_{25}) + P_{12} \Big\{ 2(P_{12} - P_{25}) \\ & - (P_{35} - P_{45}) \Big\} + P_{15}(P_{23} - P_{24}) \Big]\end{aligned}$$

$$\mathbf{T_{66}} = \mathbf{T_{55}} \left\{ \begin{array}{c} i \leftrightarrow j \\ 3 \leftrightarrow 4 \end{array} \right\}$$

$$\mathbf{T_{67}} = \mathbf{T_{58}} \left\{ \begin{array}{c} i \leftrightarrow j \\ 3 \leftrightarrow 4 \end{array} \right\}$$

$$\mathbf{T_{68}} = \mathbf{T_{57}} \left\{ \begin{array}{c} i \leftrightarrow j \\ 3 \leftrightarrow 4 \end{array} \right\}$$

$$\mathbf{T_{77}} = \frac{-16P_{14}P_{23}}{(m_i^2 - 2P_{23} - m_{\tilde{e}_h}^2)^2\,(m_j^2 - 2P_{14} - m_{\tilde{e}_h}^2)^2} \times \Big[m_i^2 + m_j^2 - 2(P_{12} - P_{13} + P_{14} + P_{23} - P_{24} + P_{34})\Big]$$

$$\mathbf{T_{78}} = \frac{16m_i m_j P_{12}\left[m_i^2+m_j^2+2(P_{12}-P_{34})\right]}{(m_i^2-2P_{23}-m_{\tilde{e}_h}^2)(m_i^2-2P_{13}-m_{\tilde{e}_h}^2)(m_j^2-2P_{14}-m_{\tilde{e}_h}^2)(m_j^2-2P_{24}-m_{\tilde{e}_h}^2)}$$

$$\mathbf{T_{88}} = \mathbf{T_{77}} \left\{ \begin{array}{c} i \leftrightarrow j \\ 3 \leftrightarrow 4 \end{array} \right\}$$

$$\begin{aligned} \mathbf{T_{st}} &= T_{13} - T_{14} + T_{15} - T_{16} + T_{17} - T_{18} \\ &\quad + T_{23} - T_{24} + T_{25} - T_{26} + T_{27} - T_{28} \\ \mathbf{T_{t1}} &= T_{33} + T_{44} + T_{55} + T_{66} + T_{77} + T_{88} \\ &\quad + T_{35} + T_{37} + T_{46} + T_{48} + T_{57} + T_{68} \\ \mathbf{T_{t2}} &= T_{34} + T_{36} + T_{38} + T_{45} + T_{47} + T_{56} + T_{58} + T_{67} + T_{78} \end{aligned}$$

$$\begin{aligned} T(\widetilde{N}_i\widetilde{N}_j) &= B_W(T_{11} + T_{12} + T_{22}) \\ &\quad + \sum_{h=L,R}\Big[B_W S\Big\{(a_i)_h(a_j)_h T_{st}\Big\} + \Big\{(a_i)_h(a_j)_h\Big\}^2 T_{t1} \\ &\qquad + C_{ij}S_{ij}\Big\{(a_i)_h(a_j)_h\Big\}^2 T_{t2}\Big] \end{aligned}$$

where

$$\begin{aligned} G_A &= N'_{i3}N'_{j3} - N'_{i4}N'_{j4} \\ (a_i)_L &= (0.5 + S_W^2)N'_{i2} - S_W C_W N'_{i1} \\ (a_i)_R &= -S_W^2 N'_{i2} + S_W C_W N'_{i1} \\ (a_j)_L &= (0.5 + S_W^2)N'_{j2} - S_W C_W N'_{j1} \\ (a_j)_R &= -S_W^2 N'_{j2} + S_W C_W N'_{j1} \end{aligned}$$

where the matrix N' diagonalises the 4×4 neutralino mass matrix following the convention of Haber and Kane [1].

The Chiral Rotation Factor (C_{ij}) and the Fermi statistics Factor (S_{ij}) are defined as follows:

$$\begin{aligned} C_{ij} &= +1 \quad for\ \ m_{\tilde{N}_1}, m_{\tilde{N}_2} > 0 \\ &= -1 \quad for\ \ either\ \ m_{\tilde{N}_1}\ or\ m_{\tilde{N}_2} < 0 \\ S_{ij} &= +1 \quad for\ \ i \neq j \\ &= -1 \quad for\ \ i = j \end{aligned}$$

Acknowledgements. The authors wish to thank Prof. D.Roy, Jadavpur University for help in computation. They also wish to thank the organizers of the Workshop on High Energy Physics Phenomenology (WHEPP4), held in Calcutta in January 1996, where this work was discussed and Manuel Drees for valuable comments. Amitava Datta's work is supported by the Department of Science and Technology, Government of India, Project No. SP/S2/K-07/92. The work of Aseshkrishna Datta has been supported by the Council for Scientific and Industrial Research, India. Sreerup Raychaudhuri acknowledges the grant of a project (DO No. SR/SY/P-08/92) of the Department of Science and Technology, Government of India.

References

1. For reviews see, for example, H.P. Nilles, Phys. Rep. **110** (1984), 1; P. Nath, R. Arnowitt and A. Chamseddine, Applied N = 1 Supergravity, ICTP Series in Theo. Phys., Vol I, World Scientific (1984); H. Haber and G. Kane, Phys. Rep. **117**, 75 (1985); S.P. Misra, Introduction to Supersymmetry and Supergravity, Wiley Eastern, New Delhi (1992)
2. A. Datta, B. Mukhopadhyaya and M. Guchhait, Mod. Phys. Lett., **10**, 1011 (1995)
3. Some apsects of VLSPs in the context of SUSY searches at hadron colliders have been considered by H. Baer, C. Kao and X. Tata, Phys. Rev. **D48**, R2978 (1993); R.M. Barnett, J. Gunion and H. Haber, Phys. Lett. **B315**, 349 (1993)
4. CDF collaboration, F. Abe et al., Phys. Rev. Lett. **69**, 3439 (1992). D0 collaboration, S. Abachi et al, Phys. Rev. Lett. **75**, 619 (1995)
5. S. Chakraborty, A. Datta and M. Guchait, Z.Phys. **C68**,325 (1995)
6. A. Datta, Aseshkrishna Datta and S. Raychaudhuri, Phys.Lett. **B349**, 113 (1995)
7. A. Datta, M. Drees and M. Guchait, Z.Phys. **C69**, 347 (1996)
8. See, for example, H. Wachsmuth (ALEPH Collaboration), talk presented at the Workshop on High Energy Physics Phenomenology-4, Calcutta, India, January 2-14, 1996 (to appear in the proceedings); The L3 Collaboration: M. Acciari et al, CERN - PPE/96 - 29; The OPAL Collaboration: G. Alexander et al, Phys. Lett. **B377**, 181 (1996); The ALEPH Collaboration: D. Buskulic et al, Phys. Lett. **B373**, 246 (1996); The DELPHI Collaboration: P. Abreu et al, Phys. Lett. **B387**, 651 (1996)
9. H. Baer, M. Drees, X. Tata, Phys. Rev. **D41**, 3414 (1990); G. Bhattacharyya, A. Datta, S. N. Ganguli and A. Raychaudhuri, Phys. Rev. Lett. **64**, 2870 (1990); A. Datta, M. Guchhait and A. Raychaudhuri, Z. Phys. **C54**, 513 (1992); J. Ellis, G. Ridolfi and F. Zwirner, Phys. Lett. **B237**, 923 (1990); M. Davier in Proc. Joint International Lepton-Photon and Europhysics Conference in High Energy Physics, Geneva, 1992 (eds. S. Hegarty et al., World Scientific, 1992) p151
10. K.J.F. Gaemers, R. Gastmans and F.M. Renard, Phys. Rev. **D19**, 1605 (1979); M. Caffo, R. Gatto and E. Remiddi, Nucl. Phys. **B286**, 293 (1986)
11. F.A. Berends et al, Nucl. Phys. **B301**, 583 (1988)
12. L. Bento, J.C. Romao, A. Barosso Phys. Rev. **D33**, 1488 (1986)
13. M. Chen et al, Phys. Rep., **159**, 2019 (1988)
14. C.H. Chen, M. Drees, J.F. Gunion, Phys. Rev. Lett. **76**, 2002 (1996)

15. K. Grassie and P.N. Pandita, Phys. Rev. **D30**, 22 (1984)
16. S. Ambrosanio, B. Mele, G. Montagna, O. Nicrosini, and F. Piccinini , Rome preprint, ROME1-1126/95; hep-ph/9601292
17. For a review and further references see, for example, L. Trentadue, Z Physics at LEP 1, Vol. 1 (eds. G. Altarelli et al) p129; O. Nicrosini and L. Trentadue, Phys. Lett., **B196**, 551 (1987); O. Nicrosini and L. Trentadue Nucl. Phys. **B318**, 1 (1989). G. Montagna, O. Nicrosini and F. Piccinini and L. Trentadue, Nucl.Phys. **B452**, 161 (1995)
18. See, e.g., M. Tigner in Proc. XXVII International Conference on High Energy Physics, Glasgow, 1994 (eds. P.J. Bussey and I.G. Knowles, Institute of Physics Publishing, 1994)
19. L.E. Ibanez. and G.G. Ross, Phys. Lett. **B110**, 215 (1982); L.E. Ibanez and J. Lopez, Nucl. Phys. **B233**, 511 (1984); M. Drees and M.M. Nojiri, Nucl. Phys. **B369**, 54 (1992); M. Drees, in Proceedings of the Third Workshop on High Energy Particle Physics, Madras, 1994, appeared in Pramana (supplement to Vol.45, 1995, ed. S. Uma Sankar)
20. See, e.g., Y. Kawamura, H. Murayama and M. Yamaguchi, Phys. Rev. **D51**, 1337 (1995); M. Olechowski and S. Pokorski, Phys. Lett. **B344**, 201 (1995)
21. See, e.g., H. Baer, C-H. Chen, C. Kao and X. Tata, FSU-HEP-950301(1995)
22. S.P.Martin and M.T.Vaughn, Phys.Lett. **B318**, 331 (1993); N.V.Krasnikov, Phys.Lett. **B345**, 25 (1995)
23. A. Datta, M. Guchait and N.Parua, hep-ph/9609413 (to appear in Phys. Lett. **B**)